Housing environment bilaterally alters transcriptomic profile in the rat hippocampal CA1 region

Short title: Transcriptomic profiles of the left and right hippocampal CA1 regions

Azusa Kubota[1], Kentaro Kojima[2], Shinnosuke Koketsu[3], Takayuki Kannon[2,4], Takehiro Sato[2,5], Kazuyoshi Hosomichi[2,6], Yoshiaki Shinohara[7*], Atsushi Tajima[1,2*]

[1] Department of Bioinformatics and Genomics, Graduate School of Advanced Preventive Medical Sciences, Kanazawa University, Kanazawa, Japan

[2] Department of Bioinformatics and Genomics, Graduate School of Medical Sciences, Kanazawa University, Kanazawa, Japan

[3] Department of Physical Therapy, Faculty of Medical Science, Nagoya Women's University, Nagoya, Japan

[4] Department of Biomedical Data Science, Fujita Health University School of Medicine, Toyoake, Japan

[5] Department of Human Biology and Anatomy, Graduate School of Medicine, University of the Ryukyu, Nishihara, Japan

[6] Laboratory of Computational Genomics, School of Life Science, Tokyo University of Pharmacy and Life Sciences, Tokyo, Japan

[7] Department of Anatomy and Systems Biology, Faculty of Medicine, University of Yamanashi, Yamanashi, Japan

*Corresponding authors

Email: atajima@med.kanazawa-u.ac.jp (AT); yoshinohara@yamanashi.ac.jp (YS)

Abstract

Brain asymmetry is a fundamental feature of neural organization. However, the molecular basis of hippocampal lateralization in response to environmental stimuli remains poorly understood. Here, we examined the transcriptomic profiles of the left and right hippocampal CA1 regions in rats reared under isolated or enriched housing conditions to elucidate hemisphere-specific responses and shared molecular adaptations. RNA-sequencing analysis revealed lateralized differences in the number and identity of differentially expressed genes, accompanied by distinct biological themes, as indicated by overrepresentation and gene set enrichment analysis. The left CA1 region was prominently engaged in pathways related to synaptic organization and mitochondrial function, whereas the right CA1 region exhibited enrichment in transcriptional regulation and RNA metabolic processes. Despite these asymmetries, co-expression and protein–protein interaction network analyses revealed shared molecular architectures. Immediate early genes formed consistent central hubs across both hemispheres, and a common Mecp2–Grin2b–Cdkl5–Tet3 protein interaction cluster was identified as a potential integrative regulatory module. Additional enrichment analysis of differentially expressed genes shared between hemispheres further highlighted conserved responses, particularly in synaptic plasticity and cell–cell communication. Together, these findings demonstrate that the left and right CA1 regions employ distinct yet partially convergent transcriptional programs to adapt to environmental stimuli. This coordinated

molecular asymmetry provides novel insights into hippocampal lateralization and its role in experience-dependent brain plasticity.

Introduction

Numerous animals and humans have left–right asymmetric brains; in humans and primates, the acquisition of higher brain functions is closely related to brain asymmetry [1,2]. Electroencephalography and functional magnetic resonance imaging are used to characterize time- and space-dependent functional differences between the left and right cerebrum of the human brain [3]. These functional differences are thought to be due to various responses to environmental stimuli, including task performance and stress exposure. Although lateral specialization of the brain has been extensively studied, the molecular factors and intricate mechanisms remain largely unknown.

Studies on hippocampal asymmetry suggest that the genetic mechanisms of visceral and brain lateralization are different. Chiral movement of the cilia induces a leftward nodal flow during embryonic development and consistently produces predictable asymmetry in the arrangement of the thoracic and abdominal organs in adulthood [4]. Normal ciliary function in wild-type mice is associated with an uneven hippocampus, and the disruption of ciliary motility leads to the randomization of organ laterality. In mice with arbitrarily inhibited ciliary movements, bilateral right isomerism occurs in the hippocampal circuitry regardless of the

original direction of organ laterality [5]. Notably, specific gene expression patterns occasionally drive molecular variations in the brain. For example, the *iv* mouse, which has a mutation in the *Lrd* (left-right dynein) gene, exhibits disrupted organ lateralization and loss of hippocampal lateralization, ultimately resulting in spatial reference and working memory deficits [6].

In rodents, the size of the synapses of the CA1 pyramidal cells varies depending on whether they receive input from the left or right CA3 pyramidal cells [7,8]. This intrinsic asymmetry is closely associated with the differential expression patterns of glutamate receptor subunits, which, in turn, correlate with synaptic size and plasticity potential. Individual environmental experiences can further modulate this inherent asymmetry. For instance, rats reared in enriched environments characterized by running wheels, tunnels, and toys exhibit increased synaptic density, specifically in the right CA1 region, along with enhanced interhemispheric gamma coherence [9]. Environmental enrichment also leads to greater dendritic complexity, maintenance of spine density, and increased branching of hippocampal CA1 pyramidal neurons in the hippocampus [10]. These findings suggest that environmental stimulation actively facilitates functional lateralization within the hippocampal circuitry through activity-dependent synaptic and dendritic reorganization. Likewise, environmental enrichment induces profound neuroanatomical and molecular changes in other hippocampal subregions [11]. In the dentate gyrus, enrichment robustly stimulates adult neurogenesis,

synaptogenesis, and survival of new neurons, while also increasing levels of neurotrophic factors and enhancing synaptic transmission. CA3, while less frequently studied, also exhibits increased synaptic plasticity and network connectivity, supporting improved pattern completion and associative memory. Furthermore, environmentally induced lateralization and plasticity are not unique to rodents. They have been observed across diverse species, including zebrafish, birds, and humans, indicating that experience-dependent brain asymmetry is a highly conserved and functionally important phenomenon [12,13]. Therefore, to fully understand the intricate mechanisms underlying neural asymmetry formation, it is essential to consider not only the structural and electrophysiological aspects, but also the dynamic, context-dependent gene expression responses of hippocampal regions to environmental stimuli.

Differential mRNA profiles between the whole left and right rat hippocampi have been observed using microarrays [14], and interhemispheric differences in miRNA profiles have been found in the rat hippocampal CA3 region [15]. Moreover, previous reports revealed that housing environments alter gene expression in the rodent brain, including the hippocampus [16-18]. However, the genes responsible for neurological laterality in the rodent hippocampus and the environmental influence on asymmetry remain unknown. Therefore, in this study, we aimed to elucidate the transcriptomic profiles of the left and right CA1 regions and to assess their respective sensitivity to an enriched environment using RNA-sequencing

(RNA-seq). Through systematic analyses of differentially expressed genes (DEGs) across hemispheric and environmental contrasts, including counts, functional enrichment, and co-expression/protein–protein interaction networks, we identified both distinct and shared molecular responses of the bilateral CA1 regions to environmental stimuli.

Materials and methods

Animals and microdissection

Male Long Evans rats were reared under either isolated (ISO) or enriched (ENR) conditions. Rats in the ISO group were caged individually after weaning at 21 days of age and raised in standard cages (length, 32 cm; width, 22 cm; height, 13.5 cm). In the ENR group, five to six male littermates were housed together in a larger cage (length, 44 cm; width, 27 cm; height, 18.7 cm) with a ladder, running wheels, tunnels, and toys, the location of which was changed every 3–4 days. Hippocampal slices were prepared, as described previously, 4 weeks after rearing under the respective environmental conditions [7,8,15]. Briefly, the rats were euthanized with isoflurane, and their brains were immediately washed with ice-cold artificial cerebrospinal fluid (ACSF). After cooling in ACSF for 15 min, hippocampal slices were cut into 400-μm-thick sections using a McIlwain tissue chopper. The bilateral rat CA1 regions were manually dissected under a stereoscopic microscope (Olympus, Tokyo, Japan) using a handmade microblade. Three biological replicates were prepared for sequencing from the left

and right CA1 regions. To minimize the effects of changes in the number of animals in the cage, ENR brain slices were prepared on the same day. The Animal Experimental Committee of Nagoya City University approved the study design (approval number: H29M-44). The animal study protocol complied with the ARRIVE guidelines 2.0 (https://arriveguidelines.org).

Library preparation and RNA-seq

Total RNA was extracted from rat CA1 region tissues using the RNeasy® Mini Kit (Qiagen, Germany), according to the manufacturer's protocol. All RNA samples exhibited an appropriate range of RNA integrity number values, as measured using a bioanalyzer (Agilent, USA). The cDNA libraries for RNA-seq were prepared from 500 ng of extracted RNA using the TruSeq® Stranded mRNA Sample Preparation Kit (Illumina, USA), according to the manufacturer's instructions. The libraries were sequenced on an Illumina HiSeq2000 to obtain 101-bp paired-end reads for each sample.

Computational quantification of gene expression

The sequenced reads were processed using fastp [19] (version 0.23.4) to eliminate low-quality reads and trim adapter sequences. Transcript quantification was performed using Salmon [20] (version 1.10.3) with Ensembl release 113 of the mRatBN7.2 cDNA assembly. Salmon output files were converted into read-count data and summarized from transcript-level to gene-level quantification using tximport [21] (version 1.34.0). The raw gene count data for downstream analyses are provided in the S1 Data. The converted raw gene count data were

normalized using tximport with the transcripts per million (TPM) method for multivariate analysis, as described below. Hierarchical clustering was conducted to summarize sample similarities based on Pearson's correlation, and multidimensional scaling was used to visualize the relationships among the samples. TPM-normalized gene count data are provided in S2 Data.

Differentially expressed genes (DEGs) analysis

Statistical analyses of DEGs were performed using edgeR [22-24] (version 4.4.2). After filtering out genes with very low expression using the edgeR::filterByexpr() function, the quasi-likelihood F-test was used to evaluate the significance of gene expression differences. An appropriate design matrix was formulated for the paired left–right sample quasi-likelihood F-test analysis. Nominal *p*-values were adjusted using false discovery rate (FDR) correction. In this step, the left group was treated as the control in the left–right comparison, and the ISO group was treated as the control in the ISO-ENR comparison. DEGs were detected using arbitrary thresholds of FDR = 0.1 and $\log_2$(fold-change) ($\log_2$FC) = $\pm\log_2 1.5$ (= ±0.58). Overlapping ISO-ENR DEGs between the left and right CA1 regions were visualized as Venn diagrams using the jvenn web application (http://bioinfo.genotoul.fr/jvenn) [25]. The primary assembly FASTA and genomic annotation GTF files of mRatBN7.2 were downloaded from Ensembl release 113.

Correlation and multivariate analysis

The $\log_2$FC values of the 14,368 common Ensembl gene IDs from housing condition comparisons of the left and right CA1 regions were used for correlation analysis. To ensure the robustness of multivariate analysis, gene-wise expression variability was quantified using the mean absolute $\log_2$FC, and the top 500 genes were selected based on this metric for heatmap generation.

Reverse transcription quantitative polymerase chain reaction (RT-qPCR)

Reverse transcription was performed using ReverTra Ace® qPCR RT Master Mix (TOYOBO, Japan). The PCR mixture was prepared with 10.0 µL of THUNDERBIRD® Next SYBR qPCR Mix (TOYOBO, Japan), 0.3 µM of forward and reverse primer, 1.0 µL of cDNA, and 7.8 µL of sterilized water. QuantStudio 6 Pro (Applied Biosystems, USA) was used for qPCR analysis. A relative quantification method [26] was used to measure the amount of each gene, with *Gapdh* as a normalizer. Details of the primer sequences used are provided in S1 Table. Welch's *t*-test was performed between the ISO and ENR groups using the ΔCq values. Click-qPCR [27] was used for the statistical analysis and visualization of gene expression.

Over-representation analysis (ORA)

ORA of ISO-ENR DEGs was conducted using g:Profiler [28] (https://biit.cs.ut.ee/gprofiler, version e113_eg59_p19_f6a03c19, database updated,

23/05/2025). Significant enrichment was tested across multiple categories, with Gene Ontology (GO) [29] (GO:Molecular Function [MF], GO:Biological Process [BP], GO:Cellular Component [CC]), Reactome [30], Kyoto Encyclopedia of Genes and Genomes (KEGG) [31], and TRANSFAC [32] as the transcription factor target databases and miRTarBase [33] as a miRNA motif database. Notably, driver GO terms were identified by grouping significant GO terms into relational clusters and selecting representative terms that explained the enrichment of the surrounding functions, whereas other emphasized terms were manually selected. The significance threshold was set at 0.05, following the g:SCS method, which adjusts *p*-values for GO enrichment by accounting for the hierarchical structure of GO terms. This approach provides a more accurate multiple testing correction than standard methods, such as the Bonferroni and Benjamini–Hochberg corrections for dependent tests. This reduces redundancy and highlights key biological themes by retaining multiple leading terms for functional groups [34].

Gene co-expression and protein–protein interaction (PPI) network analysis

DEGs identified from environmental comparisons using Ensembl gene IDs were converted to gene symbols and annotated using the g:Convert tool in g:Profiler. Next, Cytoscape [35] (version 3.10.2) and its plugins GeneMANIA [36] (application version: 3.5.3) and STRING [37] (application version: 2.2.0) were used to analyze gene co-expression and

PPI networks among the converted DEGs. In the network visualization, the size and color of each node indicate the calculated betweenness centrality in the network, with larger and more intensely colored nodes representing a relatively higher centrality. The thickness of each edge indicates the normalized maximum weight score, which reflects the strength or confidence of the association between two genes or proteins. To improve clarity, isolated nodes were manually removed from the network.

Gene set enrichment analysis (GSEA)

GSEA [38] was performed on the environmental comparison data using clusterProfiler [39-41] (version 4.14.6) and fgsea [42] (version 1.32.4), with the R package org.Rn.eg.db (version 3.20.0) used for genomic annotation. GO was used to characterize the biological features of the gene sets using the clusterProfiler:gseGO() function. To enhance the interpretability of the enrichment analysis, the Molecular Signatures Database (MSigDB) [43] and its R package msigdbr (version 24.1.0) were used for pathway enrichment analysis using the clusterProfiler::GSEA() function. The $\log_2$FC values calculated using edgeR were used as input, and the following parameters were specified for GSEA: minGSSize = 10, maxGSSize = 500, eps = 0, nPermSimple = 10000, pvalueCutoff = 0.1, pAdjustMethod = "BH" (Benjamini-Hochberg), and by = "fgsea." In the resulting dot plot, the GeneRatio (i.e., the ratio of core enrichment genes to the total number of genes in each gene set) was plotted on the x-axis, indicating the proportion of genes that most strongly contributed to enrichment.

In GSEA, core-enriched genes are defined as the subset of genes that contribute most significantly to the enrichment score, thereby representing the central elements driving the biological changes within each gene set. These genes were then used to calculate the GeneRatio in the dot plot, indicating their contribution to primary changes in the pathway.

Data processing, statistics, and drawing

R (version 4.4.2) and its tidyverse package (version 2.0.0) were used for data preprocessing, statistical computing, and data visualization.

Results

Comparison of transcriptomic similarities

Transcript quantification and summarization were successfully performed, resulting in the identification of 23,978 genes; each was annotated with a unique Ensembl gene ID. The raw gene count dataset was normalized to scaled TPM values, which were used for the analyses described in this section (S1 Data). To examine the overall transcriptomic similarity between samples, multivariate analyses were conducted based on the scaled TPM values (S2 Fig). The hierarchical clustering dendrogram revealed a clear separation between the ENR and ISO groups and the left and right CA1 region samples from the same individual clustered as pairs. Furthermore, the multidimensional scaling plot based on the scaled TPM values illustrated the relative distances among the samples.

DEG analysis and RT-qPCR

DEG analysis showed that no genes met the significance criteria in the left–right comparison under the ENR conditions, whereas only one DEG, *Pklm1*, was identified under the ISO conditions (S3 Fig). The complete edgeR results for the left–right comparison are provided in S2 Data. Conversely, the ISO–ENR comparison revealed significant differences in the gene expression profiles in both the left and right CA1 regions. In the left CA1 region, 189 DEGs were identified: 25 genes were highly expressed in the ENR group, and 164 genes were highly expressed in the ISO group (Fig 1A). In the right CA1 region, 94 DEGs were detected: 13 genes were highly expressed in the ENR group and 81 genes in the ISO group (Fig 1B). The full edgeR results for the ISO–ENR comparison are available in the S3 Data, and the corresponding DEG lists are compiled in the S4 Data.

Fig 1. Differentially expressed genes (DEGs) in the housing condition comparison between the left and right CA1 regions. (A) and (B) show volcano plots illustrating the distribution of statistically tested genes. FDR: false discovery rate; FC: fold-change. Thresholds for DEG analysis (FDR = 0.1 and $\log_2 FC = \pm \log_2 1.5$) are indicated using green dashed lines. (A) ISO–ENR comparison in the left CA1 region. (B) ISO–ENR comparison in the right CA1 region. ISO, isolated housing conditions; ENR, enriched housing conditions.

The number of overlapping ISO–ENR DEGs between the left and right CA1 regions was visualized using Venn diagrams (Fig 2A). A total of 70 DEGs were shared, with seven upregulated in the ENR group and 63 upregulated in the ISO group. All shared DEGs are listed in Table 1. To validate the DEG analysis results, RT-qPCR experiments were carried out using the selected genes from Table 1 according to the following criteria: $\log_{10}$CPM > 3 and FDR < 0.05. Among the genes that met these criteria, *Cdkl5* and *Fos* genes were selected for RT-qPCR analysis. *Cdkl5* and *Fos* showed significantly lower relative expression in the ENR group than in the ISO group in both the left and right CA1 regions (Figs 2B and 2C).

Fig 2. Summary of bilaterally shared ISO–ENR DEGs and RT-qPCR validation. (A) Venn diagrams showing the overlap between the ISO–ENR DEG sets in the left and right CA1 regions. (B) RT-qPCR quantification of *Fos* and *Cdkl5* expression, normalized to *Gapdh*. *p < 0.05, **p < 0.01, ***p < 0.001. ISO, isolated housing conditions; ENR, enriched housing conditions; DEGs, differentially expressed genes; RT-qPCR, reverse transcription-quantitative polymerase chain reaction.

Table 1. Shared DEGs by comparing rearing environments in bilateral CA1.

Gene	Description	logFC (L)	logCPM (L)	FDR (L)	logFC (R)	logCPM (R)	FDR (R)
Abca5	ATP binding cassette subfamily A member 5	-2.600	1.191	0.066	-9.905	1.185	0.014
Adgrf5	adhesion G protein-coupled receptor F5	-0.697	3.738	0.089	-0.919	3.630	0.032
Ago3	argonaute RISC catalytic component 3	-0.750	3.282	0.037	-0.653	3.294	0.026
Ankrd52	ankyrin repeat domain 52	-0.695	4.779	0.003	-0.596	4.785	0.048
Apold1	apolipoprotein L domain containing 1	-1.702	2.150	0.023	-2.317	2.306	0.023
Arfgef3	ARFGEF family member 3	-0.588	5.949	0.009	-0.629	5.886	0.016
Bach2	BTB domain and CNC homolog 2	-0.803	1.885	0.052	-0.772	1.879	0.056
Bmp3	bone morphogenetic protein 3	-0.684	2.255	0.070	-1.332	2.081	0.038
Btg2	BTG anti-proliferation factor 2	-1.224	2.917	0.013	-1.244	2.908	0.026
Cacna1e	calcium voltage-gated channel subunit alpha1 E	-0.891	7.262	0.002	-0.832	7.217	0.015
Caln1	calneuron 1	-0.728	4.474	0.005	-0.778	4.363	0.039
Cbl	Cbl proto-oncogene	-0.714	4.648	0.004	-0.690	4.675	0.018
Cchcr1	coiled-coil alpha-helical rod protein 1	0.829	2.310	0.025	0.821	2.174	0.081
Cdkl5	cyclin-dependent kinase-like 5	-0.840	5.585	0.003	-0.769	5.549	0.014
Cds2	CDP-diacylglycerol synthase 2	-0.662	5.235	0.010	-0.737	5.171	0.014
Clmn	calmin	-0.724	5.496	0.005	-0.639	5.435	0.032
Csrnp3	cysteine and serine rich nuclear protein 3	-0.781	4.124	0.007	-0.602	4.129	0.099
Dgkh	diacylglycerol kinase, eta	-1.414	3.131	0.003	-0.931	3.096	0.086
Egfr	epidermal growth factor receptor	-0.748	2.294	0.096	-0.790	2.227	0.068
Egr2	early growth response 2	-1.455	2.856	0.006	-1.673	2.710	0.036
Elfn2	extracellular leucine-rich repeat and fibronectin type III domain containing 2	-0.917	7.317	0.006	-0.832	7.217	0.032
Erbb4	erb-b2 receptor tyrosine kinase 4	-1.030	3.940	0.013	-0.757	3.845	0.014
Flt1	Fms related receptor tyrosine kinase 1	-0.676	4.561	0.089	-0.882	4.485	0.073

Gene	Description	logFC (L)	logCPM (L)	FDR (L)	logFC (R)	logCPM (R)	FDR (R)
Fos	Fos proto-oncogene, AP-1 transcription factor subunit	-1.835	3.075	0.002	-1.876	3.045	0.009
Fzd3	frizzled class receptor 3	-0.656	4.324	0.014	-0.597	4.313	0.018
Gabrb1	gamma-aminobutyric acid type A receptor subunit beta1	-0.839	4.376	0.010	-0.825	4.264	0.014
Gan	gigaxonin	-1.038	1.889	0.026	-1.137	1.829	0.060
Grin2a	glutamate ionotropic receptor NMDA type subunit 2A	-0.932	7.760	0.002	-0.717	7.752	0.032
Grin2b	glutamate ionotropic receptor NMDA type subunit 2B	-1.411	5.835	0.0004	-1.123	5.771	0.005
Gucy1a2	guanylate cyclase 1 soluble subunit alpha 2	-1.066	2.955	0.007	-1.007	3.005	0.014
Hivep3	HIVEP zinc finger 3	-0.681	5.667	0.006	-0.587	5.594	0.067
Igsf9b	immunoglobulin superfamily, member 9B	-1.368	2.790	0.002	-1.083	2.644	0.051
Ino80d	INO80 complex subunit D	-1.175	2.272	0.004	-1.025	2.323	0.024
Junb	JunB proto-oncogene, AP-1 transcription factor subunit	-0.745	5.479	0.004	-0.788	5.419	0.018
Kdr	kinase insert domain receptor	-0.923	2.770	0.091	-1.324	2.725	0.057
Klf10	KLF transcription factor 10	-0.603	5.020	0.020	-0.652	5.014	0.038
Mecp2	methyl CpG binding protein 2	-0.836	3.695	0.003	-0.764	3.624	0.039
Mrtfb	myocardin related transcription factor B	-0.655	6.576	0.005	-0.617	6.494	0.032
Mtcl2	microtubule crosslinking factor 2	-0.953	4.782	0.003	-0.758	4.723	0.051
Npas4	neuronal PAS domain protein 4	-1.267	2.819	0.070	-1.429	2.877	0.090
Nsd3	nuclear receptor binding SET domain protein 3	-0.755	4.227	0.004	-0.753	4.185	0.014
Pdzrn4	PDZ domain containing RING finger 4	-1.111	1.705	0.015	-0.973	1.732	0.065
Phc3	polyhomeotic homolog 3	-0.732	3.975	0.004	-0.615	3.983	0.043
Ppp1r9a	protein phosphatase 1, regulatory subunit 9A	-0.625	6.169	0.003	-0.604	6.112	0.014
Ptar1	protein prenyltransferase alpha subunit repeat containing 1	-0.931	2.587	0.007	-0.806	2.737	0.027
Ptprb	protein tyrosine phosphatase, receptor type, B	-0.695	4.413	0.084	-0.947	4.258	0.086
Rc3h1	ring finger and CCCH-type domains 1	-0.662	3.984	0.007	-0.593	3.936	0.032

Gene	Description	logFC (L)	logCPM (L)	FDR (L)	logFC (R)	logCPM (R)	FDR (R)
RT1-CE15	RT1 class I, locus CE15	-2.765	1.491	0.024	-4.398	1.570	0.015
RT1-CE16	RT1 class I, locus CE16	0.770	4.842	0.010	0.844	4.844	0.014
RT1-N1	RT1 class Ib, locus N1	1.451	2.212	0.003	1.430	2.082	0.014
RT1-N3	RT1 class Ib, locus N3	1.024	1.610	0.010	1.170	1.582	0.034
Scn8a	sodium voltage-gated channel alpha subunit 8	-0.720	7.846	0.002	-0.679	7.784	0.014
Slc1a2	solute carrier family 1 member 2	-0.836	9.126	0.003	-0.762	9.074	0.043
Slc4a8	solute carrier family 4 member 8	-0.834	4.395	0.004	-0.750	4.283	0.051
Slc7a14	solute carrier family 7, member 14	-0.623	4.700	0.004	-0.602	4.645	0.042
Ston2	stonin 2	-0.796	4.162	0.004	-0.881	4.052	0.038
Tanc2	tetratricopeptide repeat, ankyrin repeat and coiled-coil containing 2	-0.714	6.028	0.002	-0.618	5.989	0.030
Tead1	TEA domain transcription factor 1	-0.647	2.047	0.042	-0.841	1.952	0.066
Tet3	tet methylcytosine dioxygenase 3	-0.863	4.300	0.003	-0.727	4.165	0.032
Tmem245	transmembrane protein 245	-0.609	4.184	0.032	-0.857	4.199	0.026
Tnrc6b	trinucleotide repeat containing adaptor 6B	-1.121	4.268	0.002	-0.918	4.229	0.014
Xkr4	XK related 4	-0.648	4.784	0.013	-0.668	4.755	0.014
Zbtb20	zinc finger and BTB domain containing 20	-1.572	3.396	0.002	-1.178	3.305	0.015
Zfp704	zinc finger protein 704	-1.001	3.440	0.004	-0.794	3.400	0.043
ENSRNOG00000066523	None	1.330	3.232	0.013	1.397	3.164	0.027
ENSRNOG00000066876	None	-0.991	1.982	0.071	-1.279	1.981	0.014
ENSRNOG00000067970	None	-1.034	2.914	0.011	-0.911	2.874	0.065
ENSRNOG00000069024	None	-0.908	3.174	0.026	-1.060	3.201	0.047
ENSRNOG00000069624	None	1.712	1.187	0.039	1.280	0.904	0.049
ENSRNOG00000070648	None	0.842	5.558	0.028	0.964	5.551	0.053

logCPM, $\log_{10}$CPM; logFC, $\log_2$(fold-change); FDR, false discovery rate. L: left, R: right; DEGs, differentially expressed genes.

To further characterize the ISO–ENR DEGs, correlation and multivariate analyses were conducted using $\log_2$FC values from the edgeR analysis of the left and right CA1 regions (S4 Fig). The correlation plot of the $\log_2$FC values for environmental comparisons between the left and right CA1 regions yielded a Pearson correlation coefficient of 0.587. Additionally, a heatmap based on the top 500 genes ranked by absolute $\log_2$FC values showed a high degree of directional similarity in gene expression in the bilateral CA1 regions.

ORA of bilateral DEGs in the environmental comparison

To elucidate the biological significance of the effects of the housing environment on bilateral CA1 regions, ORA was performed using the ISO–ENR DEGs identified in the left and right hippocampal CA1 regions. All results obtained using g:Profiler are provided in the S5 Data.

Fig 3A shows the functional associations of the DEGs in the left hippocampal CA1 region as determined with GO enrichment and pathway analyses. A total of 189 DEGs were analyzed based on Ensembl gene IDs, of which 180 were annotated. This analysis revealed significant enrichment of GO-MF terms related to gene transcription and DNA binding (e.g., sequence-specific DNA binding and DNA-binding transcription factor activity), as well as membrane-associated protein functions (e.g., transmembrane signaling receptor activity, voltage-gated ion channel activity, and glutamate-gated calcium ion channel activity). Among

BP terms, those associated with nervous system development (e.g., axonogenesis), synaptic function, and memory formation (e.g., long-term memory and synaptic vesicle localization) were identified. For CC, synapse- and axon-related terms (e.g., synaptic membrane, Schaffer collateral-CA1 synapse, and axon initial segment) were significantly enriched. Pathway analysis indicated significant enrichment of the MAPK signaling pathway (KEGG:04010) and the nuclear receptor transcription pathway (REAC:R-NOR-383280).

Fig 3. Manhattan plots showing significantly enriched terms from over-representation analyses of the left and right ISO–ENR DEGs. The numbered and emphasized points have the following characteristics: Driver terms, representing the most relevant GO terms in a tabular format, are highlighted in GO:MF, GO:BP, and GO:CC. Other highlighted points were manually selected based on their significance in additional databases (KEGG Pathway, REAC: Reactome Pathway, TF: TRANSFAC, and MIRNA: miRTarBase). The adjusted *p*-values (p_{adj}) were calculated using the G:SCS method implemented in g:Profiler. The threshold for statistical significance was set at 0.05. (A) Manhattan plot and the highlighted term details for the left ISO–ENR DEGs. (B) Right ISO-ENR Manhattan plot and the highlighted term details for the right ISO–ENR DEGs. ISO, isolated housing conditions; ENR, enriched housing conditions; DEGs, differentially expressed genes; GO, Gene

Ontology; MF, Molecular function; BP, Biological process; CC, Cellular component; KEGG, Kyoto Encyclopedia of Genes and Genomes.

Fig 3B shows the functional associations of the DEGs identified in the right hippocampal CA1 region using GO enrichment and pathway analyses. A total of 94 DEGs were analyzed based on Ensembl gene IDs, of which 87 were annotated. This analysis revealed significant enrichment of transmembrane receptor protein kinase activity and DNA methylation-related GO-MF terms (e.g., DNA 5-methylcytosine dioxygenase activity). In GO-BP, the regulation of RNA metabolic processes was highly enriched. For GO-CC, the terms related to cell junctions and postsynaptic density were significantly represented. Pathway analysis revealed significant enrichment of NPAS4-mediated transcriptional regulation.

Fig 4 illustrates the functional associations between shared DEGs identified through GO enrichment and pathway analyses. From the 70 shared Ensembl gene IDs, 64 corresponding annotated gene symbols were used in this analysis. This analysis revealed significant enrichment in GO-MF terms related to transcriptional regulator activity and transmembrane receptor protein tyrosine kinase activity. In terms of GO-BP, the most significantly enriched term was positive regulation of nucleobase-containing compound metabolic processes, with the smallest adjusted *p*-value. The presynaptic membrane and

receptor complex were significantly represented in GO-CC. Pathway analysis revealed significant enrichment in the calcium signaling pathway (KEGG:04020) and post-transcriptional silencing by small RNAs (REAC:R-RNO-426496). Additionally, the transcription factor E2F and microRNA miR-132-3p were found to be enriched.

Fig 4. Manhattan plot showing significantly enriched terms from over-representation analysis of the bilaterally shared ISO-ENR DEGs. The numbered and emphasized points have the following characteristics: Driver terms, representing the most relevant GO terms in a tabular format, are highlighted in GO:MF, GO:BP, and GO:CC. Other highlighted points were manually selected based on their significance in additional preset databases (KEGG Pathway, REAC: Reactome Pathway, TF: TRANSFAC, and MIRNA: miRTarBase). The adjusted *p*-values (p_{adj}) were calculated using the G:SCS method implemented in g:Profiler. The threshold for statistical significance was set at 0.05. ISO, isolated housing conditions; ENR, enriched housing conditions; DEGs, differentially expressed genes; GO, Gene Ontology; MF, Molecular function; BP, Biological process; CC, Cellular component; KEGG, Kyoto Encyclopedia of Genes and Genomes.

Gene co-expression and PPI networks of DEGs in the environmental comparison

To evaluate the functional associations among ISO–ENR DEGs, gene co-expression network analyses were performed under three different conditions: left, right, and shared ISO–ENR DEGs. Gene co-expression networks were constructed using the GeneMANIA database in Cytoscape (Figs 5A, 6A, and 7A). All results from the Cytoscape analysis are provided in S6 Data. To highlight the common features of the bilaterally shared DEGs, highly correlated genes were predicted and visualized using a query gene-based weighting algorithm (Fig 7A). Across the three co-expression networks, a cluster of immediate early genes (IEGs), such as *Arc*, *Fos*, and *Junb*, was connected by thick edges. Additionally, key hub DEGs were highlighted in each network: *Shc3*, *Tnr*, and *Taok1* in the left CA1 region; *Ppp1r9a* and *Erbb4* in the right CA1 region; *Ppp1r9a*, *Jun*, and *Fosb* in the shared DEGs.

Fig 5. Gene co-expression and protein–protein interaction networks of the left CA1 region DEGs in the ISO-ENR comparison. A total of 180 DEGs annotated with gene symbols were included in the analysis. In network visualization, node size and color represent betweenness centrality, with larger and more intensely colored nodes indicating higher centrality. Edge thickness represents the normalized maximum weight score, which reflects the strength of the association between connected genes or proteins. Isolated nodes were manually excluded to ensure visual clarity. (A) Gene co-expression network constructed using the GeneMANIA database. (B) Protein–protein interaction network constructed using

the STRING database. ISO, isolated housing conditions; ENR, enriched housing conditions; DEGs, differentially expressed genes.

Fig 6. Gene co-expression and protein–protein interaction networks of the right CA1 region DEGs in the ISO-ENR comparison. A total of 87 DEGs annotated with gene symbols were included in the analysis. In network visualization, node size and color represent betweenness centrality, with larger and more intensely colored nodes indicating higher centrality. Edge thickness represents the normalized maximum weight score, which reflects the strength of the association between connected genes or proteins. Isolated nodes were manually excluded to ensure visual clarity. (A) Gene co-expression network constructed using the GeneMANIA database. (B) Protein-protein interaction network constructed using the STRING database. ISO, isolated housing conditions; ENR, enriched housing conditions; DEGs, differentially expressed genes.

Fig 7. Gene co-expression and protein–protein interaction networks of bilaterally shared ISO-ENR DEGs. A total of 64 DEGs annotated with gene symbols were included in the analysis. In network visualization, node size and color represent betweenness centrality, with larger and more intensely colored nodes indicating higher centrality. Edge thickness represents the normalized maximum weight score, which reflects the strength of the

association between connected genes or proteins. Isolated nodes were manually excluded to ensure visual clarity. (A) Gene co-expression network constructed using the GeneMANIA database. A query gene-based weighting algorithm was applied to highlight highly correlated genes (marked with red borders) within the network, thereby emphasizing common features among shared DEGs. (B) Protein–protein interaction network constructed using the STRING database. ISO, isolated housing conditions; ENR, enriched housing conditions; DEGs, differentially expressed genes.

To examine interactions at the protein level, PPI network analyses were also conducted under the same three conditions. PPI networks were generated using the STRING database in Cytoscape (Figs 5B, 6B, and 7B). In these networks, Fos consistently appeared as a central hub protein. In addition to the IEG protein cluster, PPI network analysis revealed strong connections that were not observed in the co-expression networks, including Fos–Npas4, Grin2a–Grin2b–Slc1a2, and Grin2b–Mecp2–Cdkl5–Tet3.

GSEA in the environmental comparison

To biologically interpret the transcriptomic alterations, gene lists ranked by their corresponding $\log_2$FC values were used to perform GSEA. The directionality of GO enrichment was evaluated using the $\log_2$FC values as a ranking metric. All GSEA results obtained using ClusterProfiler are provided in S7 Data. The dot plots in Fig 8 show the

GO-GSEA results focusing on the environmental conditions in the left and right CA1 regions. The analyses identified core enrichment genes, defined as the subset of genes that contributed most significantly to the enrichment score and potentially act as key drivers of the biological changes within each gene set (see S7 Data).

Fig 8. Biological profiles of environmental conditions based on gene set enrichment analysis (GSEA). In the ISO–ENR comparison, GSEA using Gene Ontology terms was conducted with $\log_2$(fold change) values from the edgeR analysis as input. Adjusted *p*-values are shown below each dot. The x-axis of the dot plot represents GeneRatio, which is defined as the proportion of genes within a gene set that belong to the core enrichment subset. (A) Dot plot for the left ISO–ENR. (B) Dot plot for the right ISO–ENR. ISO, isolated housing conditions; ENR, enriched housing conditions

In total, 1,293 gene sets were enriched in the left ISO–ENR analysis. Fig 8A illustrates the GO-GSEA results for the left CA1 region, showing the top 10 gene sets ranked by GeneRatio. Gene sets related to mitochondria and their functions showed a high degree of enrichment in the activated direction, indicating enrichment under ENR conditions. In the suppressed direction, corresponding to enrichment in the ISO condition, gene sets related to synapses (e.g., asymmetric synapses, postsynaptic density) and DNA-binding transcription

activator activity were observed. Contrastingly, 496 gene sets were enriched in the right ISO–ENR analysis. Fig 8B shows the GO-GSEA results in the right CA1 region, also presenting the top 10 gene sets ranked by GeneRatio. Gene sets associated with protein folding and RNA splicing were strongly enriched under the ENR conditions. Under the ISO conditions, gene sets related to synapses and transcription activator activity were enriched, consistent with the findings in the left CA1 region. Separate analyses were conducted for the GO-BP, GO-CC, and GO-MF categories. The corresponding dot plots are presented in S5 Fig (GO-BP), S6 Fig (GO-CC), and S7 Fig (GO-MF).

Finally, pathway-based enrichment analyses were performed using MSigDB's C2 Reactome and KEGG databases to complement the GO-based results. These results are shown in Figs S8 (Reactome) and S9 (KEGG). The numbers of significant pathway gene sets are as follows: Reactome, 197 on the left and 28 on the right; and KEGG, 93 on the left and 29 on the right (S7 data). These results strengthen the GO enrichment features described above. In the ENR condition, the left CA1 region showed activation of mitochondrial respiration, and the right CA1 region showed enrichment of RNA splicing. Under the ISO conditions, both regions showed stimulations of synaptic development and function.

Discussion

This study aimed to elucidate how housing conditions influence gene expression in the hippocampal CA1 region, revealing not only distinct transcriptomic landscapes but also common molecular frameworks in the left and right hemispheres. Through comprehensive analyses of DEGs, including their numbers, enrichment profiles, and co-expression/PPI networks, we delineated both unique and shared molecular responses of the bilateral CA1 regions to environmental stimuli.

Transcriptomic landscapes of the bilateral CA1 regions in response to housing environments

In the comparison between the housing conditions, the number of DEGs in the right CA1 region was 94, whereas that in the left CA1 region was 189 (Fig 1). This suggests that the degree of gene expression changes in response to the housing environment differs markedly between the two hemispheres. To further interpret these differences, we performed an ORA on the DEGs from both the left and right hippocampal CA1 regions (ISO vs. ENR conditions), which revealed distinct biological processes and molecular mechanisms of each group. Notably, both regions were enriched in the transcription factors E2F and miR-132-3p, suggesting shared transcriptional and post-transcriptional control mechanisms in response to environmental stimuli in the CA1 region [44,45].

Despite these similarities, significant differences were observed between the two groups. In the left CA1 region, GO terms related to glutamate receptor activity, synapse

function, and long-term memory (e.g., glutamate-gated calcium ion channel activity and long-term memory), along with the MAPK signaling pathway, were significantly enriched (Fig 3A). These findings suggest that the activation of gene groups is crucial for neuroplasticity and synaptic transmission, supporting the notion that environmental stimuli predominantly activate mechanisms related to nervous system function and memory formation in the left hemisphere [46]. Conversely, the right CA1 region exhibited enrichment in pathways associated with RNA metabolism and cellular structural reorganization (e.g., regulation of RNA metabolic processes and cell periphery), as illustrated in Fig 3B. Furthermore, the pathways regulated by the neuron-specific transcription factor NPAS4, known for controlling activity-dependent gene expression [47], were enriched, highlighting responses primarily involved in intrinsic cell regulation and homeostasis and suggesting a focus on gene expression regulation in the right hemisphere response.

Next, we employed GSEA to evaluate functional trends at the gene set level in both the left and right hippocampal CA1 regions ISO–ENR groups. The results provided deeper insights into the molecular signatures of the two groups (Fig 8, S8 Fig, and S9 Fig). In the left CA1 region, metabolic activities, including the mitochondrial respiratory chain, oxidative phosphorylation, and cellular respiration, were significantly activated by environmental enrichment. These functional categories primarily focus on energy production and align with the previously observed activation of synaptic transmission, long-term memory, and MAPK

pathways (Fig 3A), suggesting that increased neural activity is linked to increased metabolic demand. In contrast, post-transcriptional regulations within the nucleus and cytoplasm, such as RNA splicing and protein refolding, were selectively activated in the right CA1 region. This finding aligns with the activation of transcription factors such as NPAS4 and E2F, as shown in Fig 3B, reflecting a central role for intracellular regulatory mechanisms in response to stimuli. Notably, we observed similar enrichment patterns of asymmetric synaptic structures and increased postsynaptic density gene sets under the ISO conditions in both the left and right CA1 regions. Social isolation during adolescence increases gene and protein expression of NR2B in the rodent hippocampus [48,49]. This trend may reflect the significantly higher expression of *Grin2b*, which encodes GluN2B (NR2B), in the bilateral ISO group.

Collectively, these ORA and GSEA results consistently demonstrate that distinct molecular mechanisms underpin the effects of environmental treatments on the left and right hippocampal CA1 regions. While the left CA1 region facilitates coordinated metabolic activity and structural remodeling, the right CA1 region selectively activates endogenous gene regulatory mechanisms, potentially suppressing experience-driven neural plasticity in response to enriched environments. These findings highlight qualitative differences in the molecular strategies employed by each hemisphere in response to environmental stimuli,

offering a detailed perspective on functional asymmetry and localized response specificity in the hippocampus.

Commonality of environment-induced differential gene expression between the left and right CA1 regions

Co-expression and PPI network analyses of environmentally responsive DEGs in the left and right CA1 regions revealed a shared molecular framework in both areas (Figs 5A, 6A, and 7A). Within the co-expression network, IEGs, such as *Fos*, *Junb*, *Egr1*, and *Btg2*, formed central clusters in both left and right CA1 regions. This suggests that rapid transcriptional responses to environmental stimuli and early memory formation are common initial responses in both hemispheres [50,51].

Beyond IEGs, in the PPI network, molecules involved in neural development and plasticity, specifically Grin2b, Mecp2, Cdkl5, and Tet3, formed functionally connected clusters in both the left and right CA1 regions (Fig 5B, 6B, and 7 B). This Grin2b–Mecp2–Cdkl5–Tet3 cluster has been implicated in the maintenance of synaptic function, epigenetic regulation, and neurodevelopmental disorders [52-54], and likely constitutes a core basis for environment-dependent gene regulation common to both the left and right CA1 regions. Indeed, our ORA results (Fig 3) showed a significant enrichment of GO items related to synaptic structure in the left CA1 region and transcriptional regulation, including DNA 5-methylcytosine activity in the right CA1 region. The network centered on

this cluster may function as a molecular interface that integrates the responses of the two hemispheres through epigenetic control-based neural regulation. The GSEA results using the Reactome Pathway partly support this speculation: the left CA1 region shows enrichment of the gene set "transcriptional regulation by MECP2" in the ISO group (S8 Fig). However, further studies are needed to confirm this hypothesis.

Furthermore, the ORA of the shared DEGs between the left and right CA1 regions in response to environmental exposure (Fig 4) revealed the enrichment of terms related to transcriptional regulation, NMDA receptor activity, synaptic structure, and cellular signaling pathways. Notably, categories such as "sequence-specific DNA binding" and "transcription regulator activity" underscore the activation of shared transcriptional networks involving IEGs such as *Fos*, *Junb*, and *Egr1*, observed in both co-expression and PPI network analyses. These results indicate the presence of a common transcriptional response module in response to environmental stimuli in both hemispheres. Enrichment of terms such as "NMDA glutamate receptor activity" and "presynaptic membrane" further supports the shared activation of neural plasticity-related pathways, consistent with the GSEA results showing synaptic-related processes. Moreover, the detection of pathways such as the "calcium signaling pathway" and the involvement of miR-132-3p—both known to be linked to activity-dependent synaptic remodeling and long-term transcriptional control

[45,55]—suggest that core molecular mechanisms are symmetrically recruited in experience-dependent circuit reorganization across the bilateral CA1 regions.

In summary, while the left and right CA1 regions employ distinct molecular strategies (e.g., structural vs. transcriptional emphasis), they may share a common foundational response. This shared basis is evident in acute IEG responses and overlapping networks integral to neuroplasticity and epigenetic regulation. Therefore, brain laterality should not be considered a complete dichotomy but rather a graded asymmetry, where diverse response patterns are superimposed on a shared core mechanism. These findings, together with earlier network-based analyses, highlight that despite hemispheric asymmetries, a conserved molecular framework likely orchestrates transcriptional and synaptic responses to environmental input.

Limitations and perspectives

Careful consideration of sex-specific differences in lateralization is required. Following a previous study, we used male rats to exclude the potential influence of female sex hormones on lateralization [9]. However, hippocampal asymmetry has also been observed in female rats [56,57]. Recent studies have revealed sex-related differences in NMDA receptor function and synaptic plasticity [58,59]. For example, estrogen modulates NMDA receptor signaling and long-term potentiation in females, whereas males may rely more on GluN2B-mediated pathways [60]. These molecular differences may underlie the distinct

patterns of hippocampal asymmetry and memory processing between sexes, highlighting the importance of including both sexes in future studies.

Although the present study used the 4-week period following weaning as the window for environmental exposure, the appropriateness of this timeframe remains unclear. Postnatal brain development, including that of the hippocampus, involves a critical period that profoundly influences learning and experience [61,62]. Previous studies on mice have also examined the relationship between the duration of environmental enrichment and subsequent structural and functional changes, as well as alterations in hippocampal gene expression [18]. To gain a more comprehensive understanding, future research should incorporate cross-sectional studies across diverse developmental stages, including old age, and longitudinal studies spanning multiple life phases.

The statistical power of the current study for detecting DEGs may be insufficient because each group included only three animals. Experimental validation using RT-qPCR was performed for some DEGs; however, more detailed and robust statistical analyses would require larger sample sizes. For example, in the left–right comparison, only one DEG, *Pkml1*, was identified in the ISO group. The limited sample size raises concerns about reduced sensitivity; therefore, it is difficult to determine based on this study alone whether the limited detection of significant genes in the left–right comparison is due to insufficient statistical power or to underlying biological factors. Additionally, to compensate for the reduced

sensitivity due to the small sample size, a less stringent statistical criterion was used for DEG detection, raising concerns about an increased false-positive rate. Thus, large-scale studies with adequate statistical power are essential for robust and reliable identification of lateralized and environment-induced gene expression profiles.

As suggested by the enrichment analysis results, future investigations on the molecular-level left–right differences should extend beyond the mRNA layer. NMDA receptor subunit genes, including *Grin2b*, contribute to neural functional diversity and precise formation and maintenance of neural circuits through splice variation arising from alternative exon usage [63]. Additionally, *Mecp2*, which was highlighted by network analysis, is involved not only in epigenetic regulation in the brain but also in the regulation of alternative splicing [64]. Furthermore, isoform-specific alterations in Mecp2 protein levels have been implicated in Rett syndrome [65]. To further advance our findings, the identification of novel isoforms through long-read sequencing technologies and the accurate quantification of splice variants using deep sequencing, together with genome-wide epigenetic profiling, is required.

Acknowledgments

The authors thank Dr. Takatoshi Ueki and Dr. Hajime Hirase for their kind advice. The authors thank Ms. Yoko Iwauchi for technical assistance. We would like to thank Editage (www.editage.jp) for English language editing.

References

1. Corballis MC. The evolution and genetics of cerebral asymmetry. Philos Trans R Soc Lond B Biol Sci. 2009;364(1519):867-79. doi: 10.1098/rstb.2008.0232. PubMed PMID: 19064358; PubMed Central PMCID: PMCPMC2666079.
2. Corballis MC. Left brain, right brain: facts and fantasies. PLoS Biol. 2014;12(1):e1001767. Epub 20140121. doi: 10.1371/journal.pbio.1001767. PubMed PMID: 24465175; PubMed Central PMCID: PMCPMC3897366.
3. Morillon B, Lehongre K, Frackowiak RS, Ducorps A, Kleinschmidt A, Poeppel D, et al. Neurophysiological origin of human brain asymmetry for speech and language. Proc Natl Acad Sci U S A. 2010;107(43):18688-93. Epub 20101018. doi: 10.1073/pnas.1007189107. PubMed PMID: 20956297; PubMed Central PMCID: PMCPMC2972980.
4. Nonaka S, Shiratori H, Saijoh Y, Hamada H. Determination of left-right patterning of the mouse embryo by artificial nodal flow. Nature. 2002;418(6893):96-9. doi: 10.1038/nature00849. PubMed PMID: 12097914.
5. Kawakami R, Dobi A, Shigemoto R, Ito I. Right isomerism of the brain in inversus viscerum mutant mice. PLoS One. 2008;3(4):e1945. Epub 20080416. doi:

10.1371/journal.pone.0001945. PubMed PMID: 18414654; PubMed Central PMCID: PMCPMC2291575.

6. Goto K, Kurashima R, Gokan H, Inoue N, Ito I, Watanabe S. Left-right asymmetry defect in the hippocampal circuitry impairs spatial learning and working memory in iv mice. PLoS One. 2010;5(11):e15468. Epub 20101117. doi: 10.1371/journal.pone.0015468. PubMed PMID: 21103351; PubMed Central PMCID: PMCPMC2984506.

7. Kawakami R, Shinohara Y, Kato Y, Sugiyama H, Shigemoto R, Ito I. Asymmetrical allocation of NMDA receptor epsilon2 subunits in hippocampal circuitry. Science. 2003;300(5621):990-4. doi: 10.1126/science.1082609. PubMed PMID: 12738868.

8. Shinohara Y, Hirase H, Watanabe M, Itakura M, Takahashi M, Shigemoto R. Left-right asymmetry of the hippocampal synapses with differential subunit allocation of glutamate receptors. Proc Natl Acad Sci U S A. 2008;105(49):19498-503. Epub 20081203. doi: 10.1073/pnas.0807461105. PubMed PMID: 19052236; PubMed Central PMCID: PMCPMC2593619.

9. Shinohara Y, Hosoya A, Hirase H. Experience enhances gamma oscillations and interhemispheric asymmetry in the hippocampus. Nat Commun. 2013;4:1652. doi: 10.1038/ncomms2658. PubMed PMID: 23552067; PubMed Central PMCID: PMCPMC3644069.

10. Feng T, Alicea C, Pham V, Kirk A, Pieraut S. Experience-Dependent Inhibitory Plasticity Is Mediated by CCK+ Basket Cells in the Developing Dentate Gyrus. J Neurosci. 2021;41(21):4607-19. Epub 20210427. doi: 10.1523/JNEUROSCI.1207-20.2021. PubMed PMID: 33906898; PubMed Central PMCID: PMCPMC8260240.

11. Biggio F, Mostallino MC, Talani G, Locci V, Mostallino R, Calandra G, et al. Social enrichment reverses the isolation-induced deficits of neuronal plasticity in the hippocampus of male rats. Neuropharmacology. 2019;151:45-54. Epub 20190329. doi: 10.1016/j.neuropharm.2019.03.030. PubMed PMID: 30935859.

12. Gunturkun O, Ocklenburg S. Ontogenesis of Lateralization. Neuron. 2017;94(2):249-63. doi: 10.1016/j.neuron.2017.02.045. PubMed PMID: 28426959.

13. Gunturkun O, Strockens F, Ocklenburg S. Brain Lateralization: A Comparative Perspective. Physiol Rev. 2020;100(3):1019-63. doi: 10.1152/physrev.00006.2019. PubMed PMID: 32233912.

14. Moskal JR, Kroes RA, Otto NJ, Rahimi O, Claiborne BJ. Distinct patterns of gene expression in the left and right hippocampal formation of developing rats. Hippocampus. 2006;16(8):629-34. doi: 10.1002/hipo.20198. PubMed PMID: 16847945.

15. Shinohara Y, Yahagi K, Kawano M, Nishiyori H, Kawazu C, Suzuki N, et al. miRNA profiling of bilateral rat hippocampal CA3 by deep sequencing. Biochem Biophys Res

Commun. 2011;409(2):293-8. Epub 20110514. doi: 10.1016/j.bbrc.2011.05.004. PubMed PMID: 21575607.

16. Rampon C, Jiang CH, Dong H, Tang YP, Lockhart DJ, Schultz PG, et al. Effects of environmental enrichment on gene expression in the brain. Proc Natl Acad Sci U S A. 2000;97(23):12880-4. doi: 10.1073/pnas.97.23.12880. PubMed PMID: 11070096; PubMed Central PMCID: PMCPMC18858.

17. Huttenrauch M, Salinas G, Wirths O. Effects of Long-Term Environmental Enrichment on Anxiety, Memory, Hippocampal Plasticity and Overall Brain Gene Expression in C57BL6 Mice. Front Mol Neurosci. 2016;9:62. Epub 20160803. doi: 10.3389/fnmol.2016.00062. PubMed PMID: 27536216; PubMed Central PMCID: PMCPMC4971077.

18. Singhal G, Morgan J, Jawahar MC, Corrigan F, Jaehne EJ, Toben C, et al. The effects of short-term and long-term environmental enrichment on locomotion, mood-like behavior, cognition and hippocampal gene expression. Behav Brain Res. 2019;368:111917. Epub 20190417. doi: 10.1016/j.bbr.2019.111917. PubMed PMID: 31004685.

19. Chen S, Zhou Y, Chen Y, Gu J. fastp: an ultra-fast all-in-one FASTQ preprocessor. Bioinformatics. 2018;34(17):i884-i90. doi: 10.1093/bioinformatics/bty560. PubMed PMID: 30423086; PubMed Central PMCID: PMCPMC6129281.

20. Patro R, Duggal G, Love MI, Irizarry RA, Kingsford C. Salmon provides fast and bias-aware quantification of transcript expression. Nat Methods. 2017;14(4):417-9. Epub 20170306. doi: 10.1038/nmeth.4197. PubMed PMID: 28263959; PubMed Central PMCID: PMCPMC5600148.

21. Soneson C, Love MI, Robinson MD. Differential analyses for RNA-seq: transcript-level estimates improve gene-level inferences. F1000Res. 2015;4:1521. Epub 20151230. doi: 10.12688/f1000research.7563.2. PubMed PMID: 26925227; PubMed Central PMCID: PMCPMC4712774.

22. Robinson MD, McCarthy DJ, Smyth GK. edgeR: a Bioconductor package for differential expression analysis of digital gene expression data. Bioinformatics. 2010;26(1):139-40. Epub 20091111. doi: 10.1093/bioinformatics/btp616. PubMed PMID: 19910308; PubMed Central PMCID: PMCPMC2796818.

23. Chen Y, Lun AT, Smyth GK. From reads to genes to pathways: differential expression analysis of RNA-Seq experiments using Rsubread and the edgeR quasi-likelihood pipeline. F1000Res. 2016;5:1438. Epub 20160620. doi: 10.12688/f1000research.8987.2. PubMed PMID: 27508061; PubMed Central PMCID: PMCPMC4934518.

24. Chen Y, Chen L, Lun ATL, Baldoni PL, Smyth GK. edgeR v4: powerful differential analysis of sequencing data with expanded functionality and improved support for small

counts and larger datasets. Nucleic Acids Res. 2025;53(2). doi: 10.1093/nar/gkaf018. PubMed PMID: 39844453; PubMed Central PMCID: PMCPMC11754124.

25. Bardou P, Mariette J, Escudié F, Djemiel C, Klopp C. jvenn: an interactive Venn diagram viewer. BMC Bioinformatics. 2014;15(1):293. Epub 20140829. doi: 10.1186/1471-2105-15-293. PubMed PMID: 25176396; PubMed Central PMCID: PMCPMC4261873.

26. Livak KJ, Schmittgen TD. Analysis of relative gene expression data using real-time quantitative PCR and the 2(-Delta Delta C(T)) Method. Methods. 2001;25(4):402-8. doi: 10.1006/meth.2001.1262. PubMed PMID: 11846609.

27. Kubota A, Tajima A. Click-qPCR: an ultra-simple tool for interactive qPCR data analysis. bioRxiv. 2025:2025.05.29.656779. doi: 10.1101/2025.05.29.656779.

28. Kolberg L, Raudvere U, Kuzmin I, Adler P, Vilo J, Peterson H. g:Profiler-interoperable web service for functional enrichment analysis and gene identifier mapping (2023 update). Nucleic Acids Res. 2023;51(W1):W207-W12. doi: 10.1093/nar/gkad347. PubMed PMID: 37144459; PubMed Central PMCID: PMCPMC10320099.

29. Gene Ontology C, Aleksander SA, Balhoff J, Carbon S, Cherry JM, Drabkin HJ, et al. The Gene Ontology knowledgebase in 2023. Genetics. 2023;224(1). doi: 10.1093/genetics/iyad031. PubMed PMID: 36866529; PubMed Central PMCID: PMCPMC10158837.

30. Milacic M, Beavers D, Conley P, Gong C, Gillespie M, Griss J, et al. The Reactome Pathway Knowledgebase 2024. Nucleic Acids Res. 2024;52(D1):D672-D8. doi: 10.1093/nar/gkad1025. PubMed PMID: 37941124; PubMed Central PMCID: PMCPMC10767911.

31. Kanehisa M, Furumichi M, Sato Y, Matsuura Y, Ishiguro-Watanabe M. KEGG: biological systems database as a model of the real world. Nucleic Acids Res. 2025;53(D1):D672-D7. doi: 10.1093/nar/gkae909. PubMed PMID: 39417505; PubMed Central PMCID: PMCPMC11701520.

32. Matys V, Kel-Margoulis OV, Fricke E, Liebich I, Land S, Barre-Dirrie A, et al. TRANSFAC and its module TRANSCompel: transcriptional gene regulation in eukaryotes. Nucleic Acids Res. 2006;34(Database issue):D108-10. doi: 10.1093/nar/gkj143. PubMed PMID: 16381825; PubMed Central PMCID: PMCPMC1347505.

33. Cui S, Yu S, Huang HY, Lin YC, Huang Y, Zhang B, et al. miRTarBase 2025: updates to the collection of experimentally validated microRNA-target interactions. Nucleic Acids Res. 2025;53(D1):D147-D56. doi: 10.1093/nar/gkae1072. PubMed PMID: 39578692; PubMed Central PMCID: PMCPMC11701613.

34. Reimand J, Kull M, Peterson H, Hansen J, Vilo J. g:Profiler--a web-based toolset for functional profiling of gene lists from large-scale experiments. Nucleic Acids Res.

2007;35(Web Server issue):W193-200. Epub 20070503. doi: 10.1093/nar/gkm226. PubMed PMID: 17478515; PubMed Central PMCID: PMCPMC1933153.

35. Shannon P, Markiel A, Ozier O, Baliga NS, Wang JT, Ramage D, et al. Cytoscape: a software environment for integrated models of biomolecular interaction networks. Genome Res. 2003;13(11):2498-504. doi: 10.1101/gr.1239303. PubMed PMID: 14597658; PubMed Central PMCID: PMCPMC403769.

36. Warde-Farley D, Donaldson SL, Comes O, Zuberi K, Badrawi R, Chao P, et al. The GeneMANIA prediction server: biological network integration for gene prioritization and predicting gene function. Nucleic Acids Res. 2010;38(Web Server issue):W214-20. doi: 10.1093/nar/gkq537. PubMed PMID: 20576703; PubMed Central PMCID: PMCPMC2896186.

37. Szklarczyk D, Kirsch R, Koutrouli M, Nastou K, Mehryary F, Hachilif R, et al. The STRING database in 2023: protein-protein association networks and functional enrichment analyses for any sequenced genome of interest. Nucleic Acids Res. 2023;51(D1):D638-D46. doi: 10.1093/nar/gkac1000. PubMed PMID: 36370105; PubMed Central PMCID: PMCPMC9825434.

38. Subramanian A, Tamayo P, Mootha VK, Mukherjee S, Ebert BL, Gillette MA, et al. Gene set enrichment analysis: a knowledge-based approach for interpreting genome-wide expression profiles. Proc Natl Acad Sci U S A. 2005;102(43):15545-50.

Epub 20050930. doi: 10.1073/pnas.0506580102. PubMed PMID: 16199517; PubMed Central PMCID: PMCPMC1239896.

39. Yu G, Wang LG, Han Y, He QY. clusterProfiler: an R package for comparing biological themes among gene clusters. OMICS. 2012;16(5):284-7. Epub 20120328. doi: 10.1089/omi.2011.0118. PubMed PMID: 22455463; PubMed Central PMCID: PMCPMC3339379.

40. Wu T, Hu E, Xu S, Chen M, Guo P, Dai Z, et al. clusterProfiler 4.0: A universal enrichment tool for interpreting omics data. Innovation (Camb). 2021;2(3):100141. Epub 20210701. doi: 10.1016/j.xinn.2021.100141. PubMed PMID: 34557778; PubMed Central PMCID: PMCPMC8454663.

41. Xu S, Hu E, Cai Y, Xie Z, Luo X, Zhan L, et al. Using clusterProfiler to characterize multiomics data. Nat Protoc. 2024;19(11):3292-320. Epub 20240717. doi: 10.1038/s41596-024-01020-z. PubMed PMID: 39019974.

42. Korotkevich G, Sukhov V, Budin N, Shpak B, Artyomov MN, Sergushichev A. Fast gene set enrichment analysis. bioRxiv. 2021:060012. doi: 10.1101/060012.

43. Liberzon A, Subramanian A, Pinchback R, Thorvaldsdottir H, Tamayo P, Mesirov JP. Molecular signatures database (MSigDB) 3.0. Bioinformatics. 2011;27(12):1739-40. Epub 20110505. doi: 10.1093/bioinformatics/btr260. PubMed PMID: 21546393; PubMed Central PMCID: PMCPMC3106198.

44. Swiss VA, Casaccia P. Cell-context specific role of the E2F/Rb pathway in development and disease. Glia. 2010;58(4):377-90. doi: 10.1002/glia.20933. PubMed PMID: 19795505; PubMed Central PMCID: PMCPMC2882865.

45. Qian Y, Song J, Ouyang Y, Han Q, Chen W, Zhao X, et al. Advances in Roles of miR-132 in the Nervous System. Front Pharmacol. 2017;8:770. Epub 20171025. doi: 10.3389/fphar.2017.00770. PubMed PMID: 29118714; PubMed Central PMCID: PMCPMC5660991.

46. Jordan JT. The rodent hippocampus as a bilateral structure: A review of hemispheric lateralization. Hippocampus. 2020;30(3):278-92. Epub 20191227. doi: 10.1002/hipo.23188. PubMed PMID: 31880377.

47. Fu J, Guo O, Zhen Z, Zhen J. Essential Functions of the Transcription Factor Npas4 in Neural Circuit Development, Plasticity, and Diseases. Front Neurosci. 2020;14:603373. Epub 20201201. doi: 10.3389/fnins.2020.603373. PubMed PMID: 33335473; PubMed Central PMCID: PMCPMC7736240.

48. Zhao X, Sun L, Jia H, Meng Q, Wu S, Li N, et al. Isolation rearing induces social and emotional function abnormalities and alters glutamate and neurodevelopment-related gene expression in rats. Prog Neuropsychopharmacol Biol Psychiatry. 2009;33(7):1173-7. Epub 20090627. doi: 10.1016/j.pnpbp.2009.06.016. PubMed PMID: 19563853.

49. Chang CH, Hsiao YH, Chen YW, Yu YJ, Gean PW. Social isolation-induced increase in NMDA receptors in the hippocampus exacerbates emotional dysregulation in mice. Hippocampus. 2015;25(4):474-85. Epub 20141105. doi: 10.1002/hipo.22384. PubMed PMID: 25348768.

50. Lara Aparicio SY, Laureani Fierro AJ, Aranda Abreu GE, Toledo Cardenas R, Garcia Hernandez LI, Coria Avila GA, et al. Current Opinion on the Use of c-Fos in Neuroscience. NeuroSci. 2022;3(4):687-702. Epub 20221219. doi: 10.3390/neurosci3040050. PubMed PMID: 39483772; PubMed Central PMCID: PMCPMC11523728.

51. Tregub PP, Komleva YK, Kukla MV, Averchuk AS, Vetchinova AS, Rozanova NA, et al. Brain Plasticity and Cell Competition: Immediate Early Genes Are the Focus. Cells. 2025;14(2). Epub 20250119. doi: 10.3390/cells14020143. PubMed PMID: 39851571; PubMed Central PMCID: PMCPMC11763428.

52. Lee S, Kim W, Ham BJ, Chen W, Bear MF, Yoon BJ. Activity-dependent NR2B expression is mediated by MeCP2-dependent epigenetic regulation. Biochem Biophys Res Commun. 2008;377(3):930-4. Epub 20081024. doi: 10.1016/j.bbrc.2008.10.082. PubMed PMID: 18952054.

53. Rao VK, Swarnaseetha A, Tham GH, Lin WQ, Han BB, Benoukraf T, et al. Phosphorylation of Tet3 by cdk5 is critical for robust activation of BRN2 during

neuronal differentiation. Nucleic Acids Res. 2020;48(3):1225-38. doi: 10.1093/nar/gkz1144. PubMed PMID: 31807777; PubMed Central PMCID: PMCPMC7026633.

54. Zito A, Lee JT. Variable expression of MECP2, CDKL5, and FMR1 in the human brain: Implications for gene restorative therapies. Proc Natl Acad Sci U S A. 2024;121(9):e2312757121. Epub 20240222. doi: 10.1073/pnas.2312757121. PubMed PMID: 38386709; PubMed Central PMCID: PMCPMC10907246.

55. Yasuda R, Hayashi Y, Hell JW. CaMKII: a central molecular organizer of synaptic plasticity, learning and memory. Nat Rev Neurosci. 2022;23(11):666-82. Epub 20220902. doi: 10.1038/s41583-022-00624-2. PubMed PMID: 36056211.

56. Diamond MC, Murphy GM, Jr., Akiyama K, Johnson RE. Morphologic hippocampal asymmetry in male and female rats. Exp Neurol. 1982;76(3):553-65. doi: 10.1016/0014-4886(82)90124-8. PubMed PMID: 7084374.

57. Wolff SC, Hruska Z, Nguyen L, Dohanich GP. Asymmetrical distributions of muscarinic receptor binding in the hippocampus of female rats. Eur J Pharmacol. 2008;588(2-3):248-50. Epub 20080409. doi: 10.1016/j.ejphar.2008.04.002. PubMed PMID: 18499095.

58. Yagi S, Galea LAM. Sex differences in hippocampal cognition and neurogenesis. Neuropsychopharmacology. 2019;44(1):200-13. Epub 20180907. doi:

10.1038/s41386-018-0208-4. PubMed PMID: 30214058; PubMed Central PMCID: PMCPMC6235970.

59. Narattil NR, Maroun M. Differential role of NMDA receptors in hippocampal-dependent spatial memory and plasticity in juvenile male and female rats. Hippocampus. 2024;34(11):564-74. Epub 20240815. doi: 10.1002/hipo.23631. PubMed PMID: 39143939.

60. Copenhaver AE, LeGates TA. Sex-Specific Mechanisms Underlie Long-Term Potentiation at Hippocampus-->Medium Spiny Neuron Synapses in the Medial Shell of the Nucleus Accumbens. J Neurosci. 2024;44(27). Epub 20240703. doi: 10.1523/JNEUROSCI.0100-24.2024. PubMed PMID: 38806250; PubMed Central PMCID: PMCPMC11223474.

61. Sakai A, Sugiyama S. Experience-dependent transcriptional regulation in juvenile brain development. Dev Growth Differ. 2018;60(8):473-82. doi: 10.1111/dgd.12571. PubMed PMID: 30368782.

62. Sakimoto Y, Shintani A, Yoshiura D, Goshima M, Kida H, Mitsushima D. A critical period for learning and plastic changes at hippocampal CA1 synapses. Sci Rep. 2022;12(1):7199. Epub 20220503. doi: 10.1038/s41598-022-10453-z. PubMed PMID: 35504922; PubMed Central PMCID: PMCPMC9065057.

63. Tumdam R, Hussein Y, Garin-Shkolnik T, Stern S. NMDA Receptors in Neurodevelopmental Disorders: Pathophysiology and Disease Models. Int J Mol Sci. 2024;25(22). Epub 20241118. doi: 10.3390/ijms252212366. PubMed PMID: 39596430; PubMed Central PMCID: PMCPMC11594297.

64. Liu Y, Whitfield TW, Bell GW, Guo R, Flamier A, Young RA, et al. Exploring the complexity of MECP2 function in Rett syndrome. Nat Rev Neurosci. 2025;26(7):379-98. Epub 20250513. doi: 10.1038/s41583-025-00926-1. PubMed PMID: 40360671.

65. Rodrigues DC, Mufteev M, Ellis J. Regulation, diversity and function of MECP2 exon and 3'UTR isoforms. Hum Mol Genet. 2020;29(R1):R89-R99. doi: 10.1093/hmg/ddaa154. PubMed PMID: 32681172; PubMed Central PMCID: PMCPMC7530521.

Supporting information

S1 Fig. Brief workflow chart of this study.

S2 Fig. Multivariate analyses using the TPM-normalized gene count data.

S3 Fig. Volcano plot visualizations of the left–right comparison.

S4 Fig. Correlation plots focusing on the $\log_2$FC values calculated using edgeR.

S5 Fig. GSEA for the environmental comparisons in the left and right CA1 regions using the GO-BP database.

S6 Fig. GSEA for the environmental comparisons in the left and right CA1 regions using the GO-CC database.

S7 Fig. GSEA for the environmental comparisons in the left and right CA1 regions using the GO-MF database.

S8 Fig. GSEA for the environmental comparisons in the left and right CA1 regions using the MSigDB's C2 Reactome Pathway database.

S9 Fig. GSEA for the environmental comparisons in the left and right CA1 regions using the MSigDB's C2 KEGG Pathway database.

S1 Data. Raw gene count data for the edgeR analysis.

S2 Data. TPM-normalized gene count data generated by tximport.

S3 Data. The edgeR calculation results of the left–right comparison.

S4 Data. The edgeR calculation results of the ISO–ENR comparison.

S5 Data. The g:Profiler calculation results of over-representation analysis.

S6 Data. The Cytoscape calculation results of network analysis.

S7 Data. The clusterProfiler calculation results of gene set enrichment analysis.

Fig 1

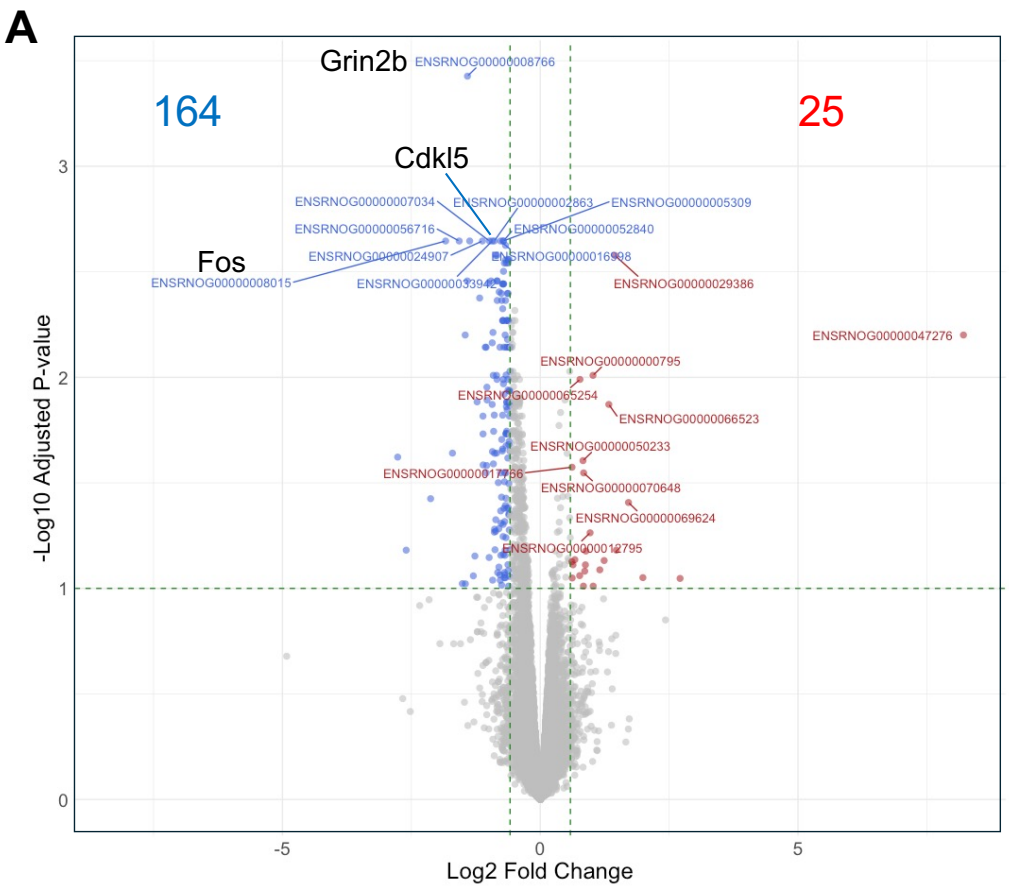

Left CA1, ISO vs ENR

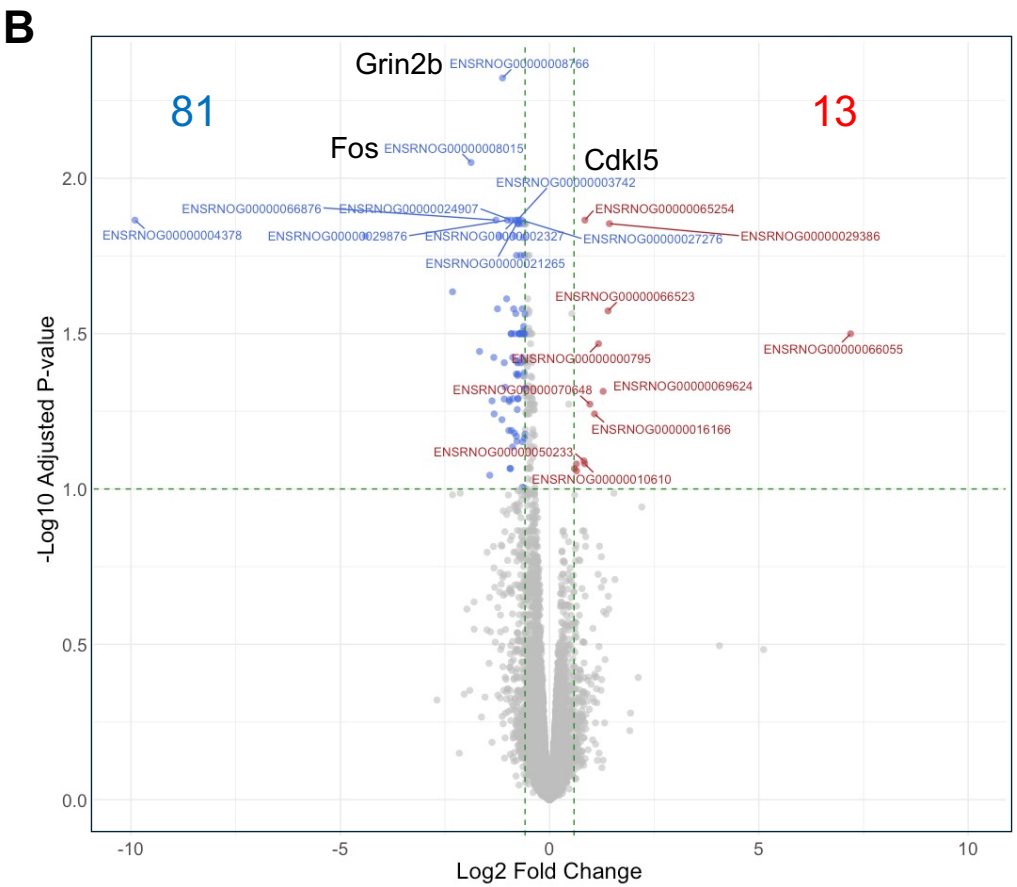

Right CA1, ISO vs ENR

Fig 2

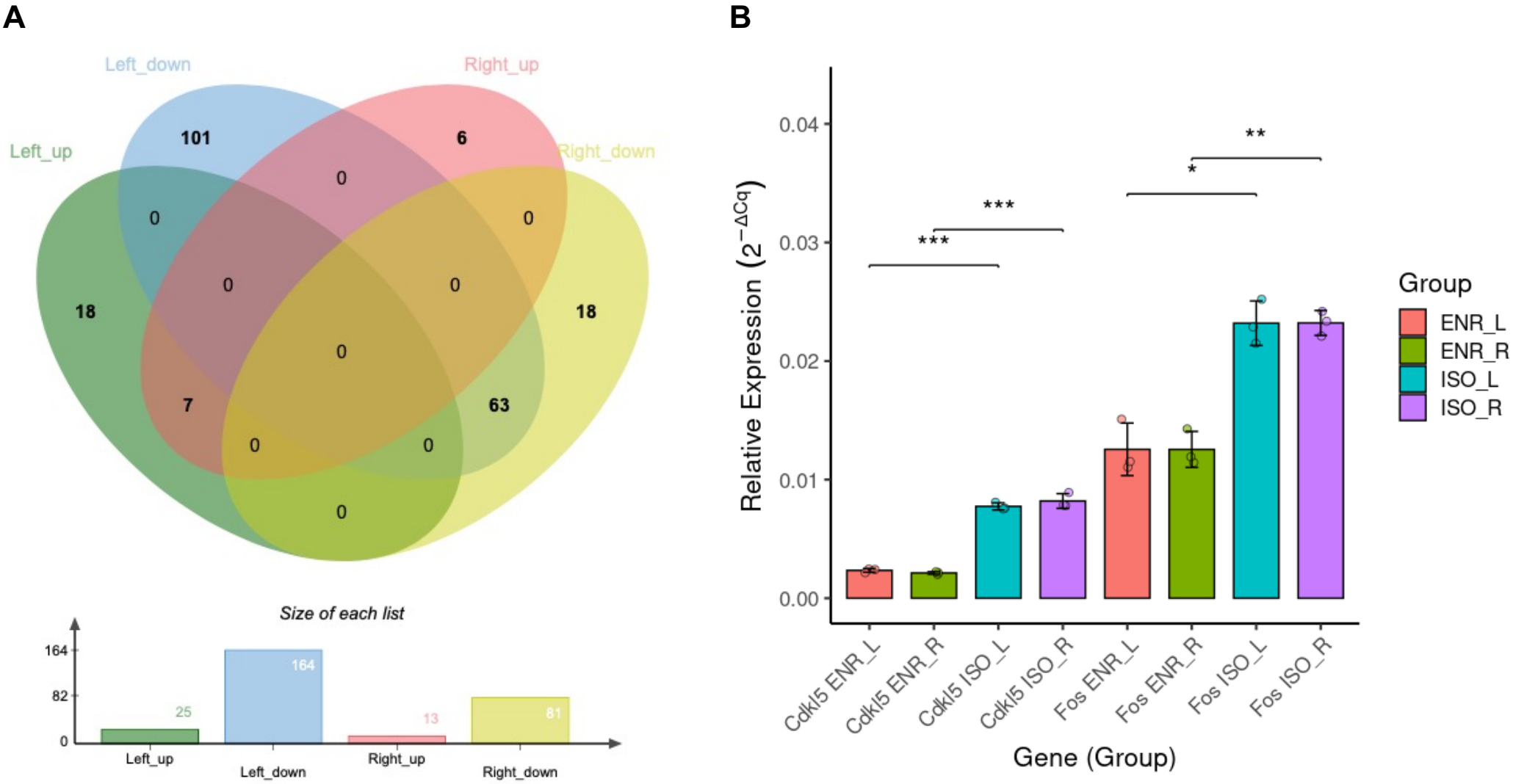
A
Left_down
Right_up
Left_up
Right_down
101
6
18
18
7
63
0
Size of each list
164
82
0
25
164
13
81
Left_up
Left_down
Right_up
Right_down
B
Relative Expression ($2^{-\Delta Cq}$)
0.04
0.03
0.02
0.01
0.00
***
***
*
**
Cdkl5 ENR_L
Cdkl5 ENR_R
Cdkl5 ISO_L
Cdkl5 ISO_R
Fos ENR_L
Fos ENR_R
Fos ISO_L
Fos ISO_R
Gene (Group)
Group
ENR_L
ENR_R
ISO_L
ISO_R

Fig 3

A

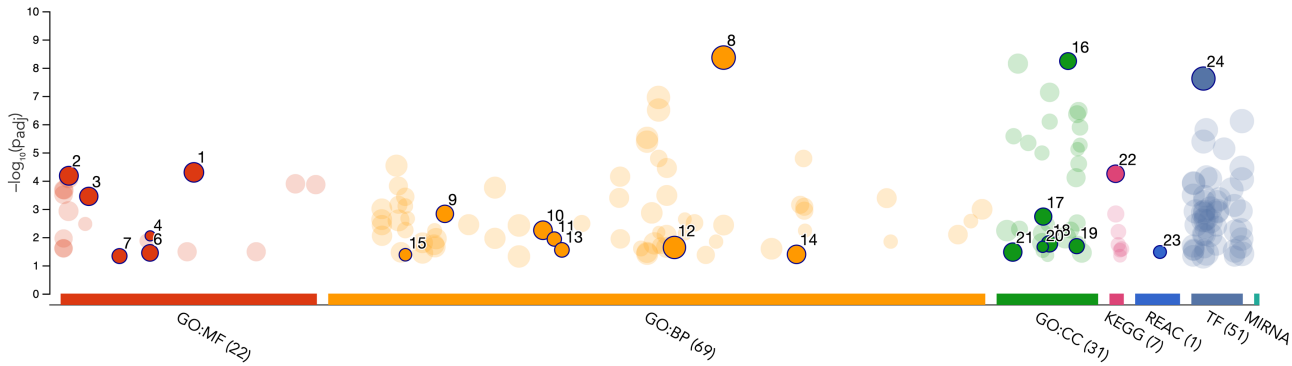

ID	Source	Term ID	Term Name	p_{adj} (query_1)
1	GO:MF	GO:0043565	sequence-specific DNA binding	5.082×10^{-5}
2	GO:MF	GO:0003700	DNA-binding transcription factor activity	6.695×10^{-5}
3	GO:MF	GO:0004888	transmembrane signaling receptor activity	3.594×10^{-4}
4	GO:MF	GO:0022849	glutamate-gated calcium ion channel activity	9.003×10^{-3}
5	GO:MF	GO:0022824	transmitter-gated monoatomic ion channel activity	3.432×10^{-2}
6	GO:MF	GO:0022836	gated channel activity	3.611×10^{-2}
7	GO:MF	GO:0015171	amino acid transmembrane transporter activity	4.677×10^{-2}
8	GO:BP	GO:0065007	biological regulation	4.369×10^{-9}
9	GO:BP	GO:0014706	striated muscle tissue development	1.496×10^{-3}
10	GO:BP	GO:0034330	cell junction organization	5.691×10^{-3}
11	GO:BP	GO:0035418	protein localization to synapse	1.167×10^{-2}
12	GO:BP	GO:0051716	cellular response to stimulus	2.319×10^{-2}
13	GO:BP	GO:0035914	skeletal muscle cell differentiation	2.828×10^{-2}
14	GO:BP	GO:0098609	cell-cell adhesion	4.073×10^{-2}
15	GO:BP	GO:0007616	long-term memory	4.203×10^{-2}
16	GO:CC	GO:0097060	synaptic membrane	5.815×10^{-9}
17	GO:CC	GO:0043235	receptor complex	1.869×10^{-3}
18	GO:CC	GO:0045121	membrane raft	1.725×10^{-2}
19	GO:CC	GO:0098685	Schaffer collateral - CA1 synapse	2.082×10^{-2}
20	GO:CC	GO:0043194	axon initial segment	2.192×10^{-2}
21	GO:CC	GO:0009986	cell surface	3.381×10^{-2}
22	KEGG	KEGG:04010	MAPK signaling pathway	5.685×10^{-5}
23	REAC	REAC:R-RNO-383280	Nuclear Receptor transcription pathway	3.362×10^{-2}
24	TF	TF:M00803_1	Factor: E2F; motif: GGCGSG; match class: 1	2.416×10^{-8}

Left ISO_ENR: Of the 189 Ensembl gene ID-based DEGs,180 annotated genes were used.

B

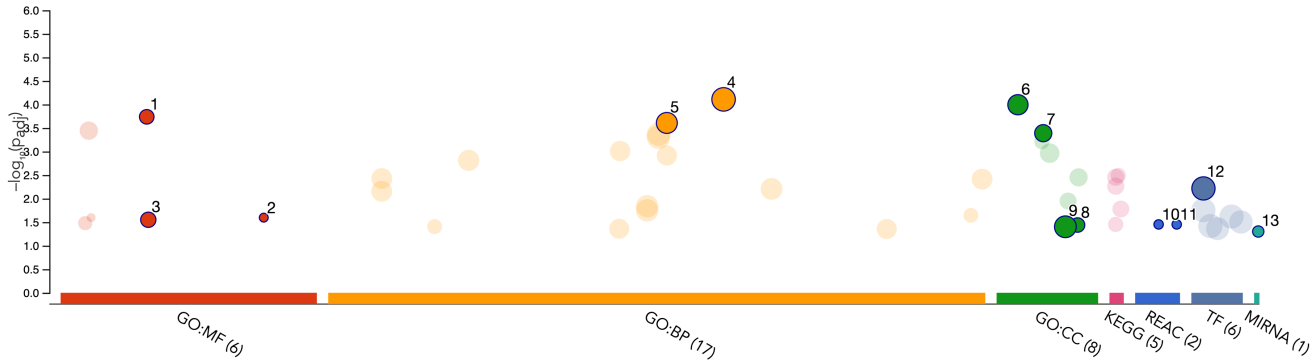

ID	Source	Term ID	Term Name	p_{adj} (query_1)
1	GO:MF	GO:0019199	transmembrane receptor protein kinase activity	1.831×10^{-4}
2	GO:MF	GO:0070579	DNA 5-methylcytosine dioxygenase activity	2.535×10^{-2}
3	GO:MF	GO:0019838	growth factor binding	2.813×10^{-2}
4	GO:BP	GO:0065007	biological regulation	7.802×10^{-5}
5	GO:BP	GO:0051252	regulation of RNA metabolic process	2.471×10^{-4}
6	GO:CC	GO:0030054	cell junction	1.014×10^{-4}
7	GO:CC	GO:0043235	receptor complex	4.075×10^{-4}
8	GO:CC	GO:0098839	postsynaptic density membrane	3.638×10^{-2}
9	GO:CC	GO:0071944	cell periphery	3.965×10^{-2}
10	REAC	REAC:R-RNO-9768919	NPAS4 regulates expression of target genes	3.533×10^{-2}
11	REAC	REAC:R-RNO-9634815	Transcriptional Regulation by NPAS4	3.533×10^{-2}
12	TF	TF:M00803_1	Factor: E2F; motif: GGCGSG; match class: 1	6.074×10^{-3}
13	MIRNA	MIRNA:rno-mir-132-3p	rno-mir-132-3p	4.999×10^{-2}

Right ISO-ENR: Of the 94 Ensembl gene ID-based DEGs, 87 annotated genes were used.

Fig 4

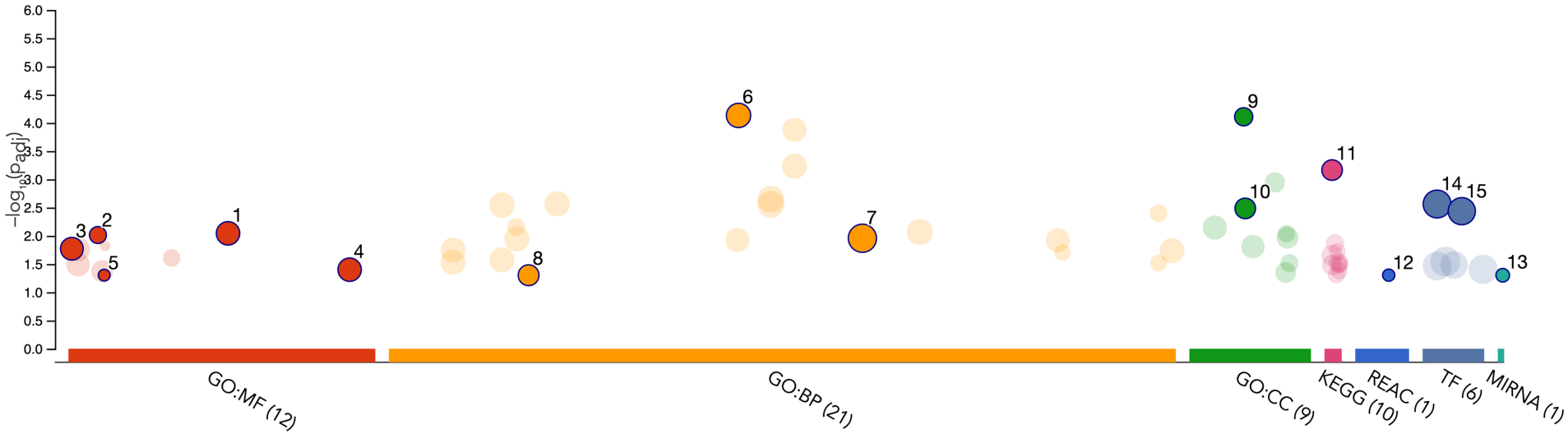

ID	Source	Term ID	Term Name	p_{adj} (query_1)
1	GO:MF	GO:0043565	sequence-specific DNA binding	9.048×10^{-3}
2	GO:MF	GO:0004714	transmembrane receptor protein tyrosine kinase activity	9.686×10^{-3}
3	GO:MF	GO:0000976	transcription cis-regulatory region binding	1.696×10^{-2}
4	GO:MF	GO:0140110	transcription regulator activity	3.982×10^{-2}
5	GO:MF	GO:0004972	NMDA glutamate receptor activity	4.988×10^{-2}
6	GO:BP	GO:0045935	positive regulation of nucleobase-containing compound metabolic process	7.383×10^{-5}
7	GO:BP	GO:0065007	biological regulation	1.105×10^{-2}
8	GO:BP	GO:0014706	striated muscle tissue development	4.992×10^{-2}
9	GO:CC	GO:0042734	presynaptic membrane	7.808×10^{-5}
10	GO:CC	GO:0043235	receptor complex	3.274×10^{-3}
11	KEGG	KEGG:04020	Calcium signaling pathway	6.858×10^{-4}
12	REAC	REAC:R-RNO-426496	Post-transcriptional silencing by small RNAs	4.979×10^{-2}
13	MIRNA	MIRNA:rno-mir-132-3p	rno-mir-132-3p	4.999×10^{-2}
14	TF	TF:M00803_1	Factor: E2F; motif: GGCGSG; match class: 1	2.737×10^{-3}
15	TF	TF:M00244	Factor: NGFI-C; motif: WTGCGTGGGYGG	3.668×10^{-3}

Of the 70 Ensembl gene IDs as shared DEGs, 64 annotated gene symbols were used.

Fig 5

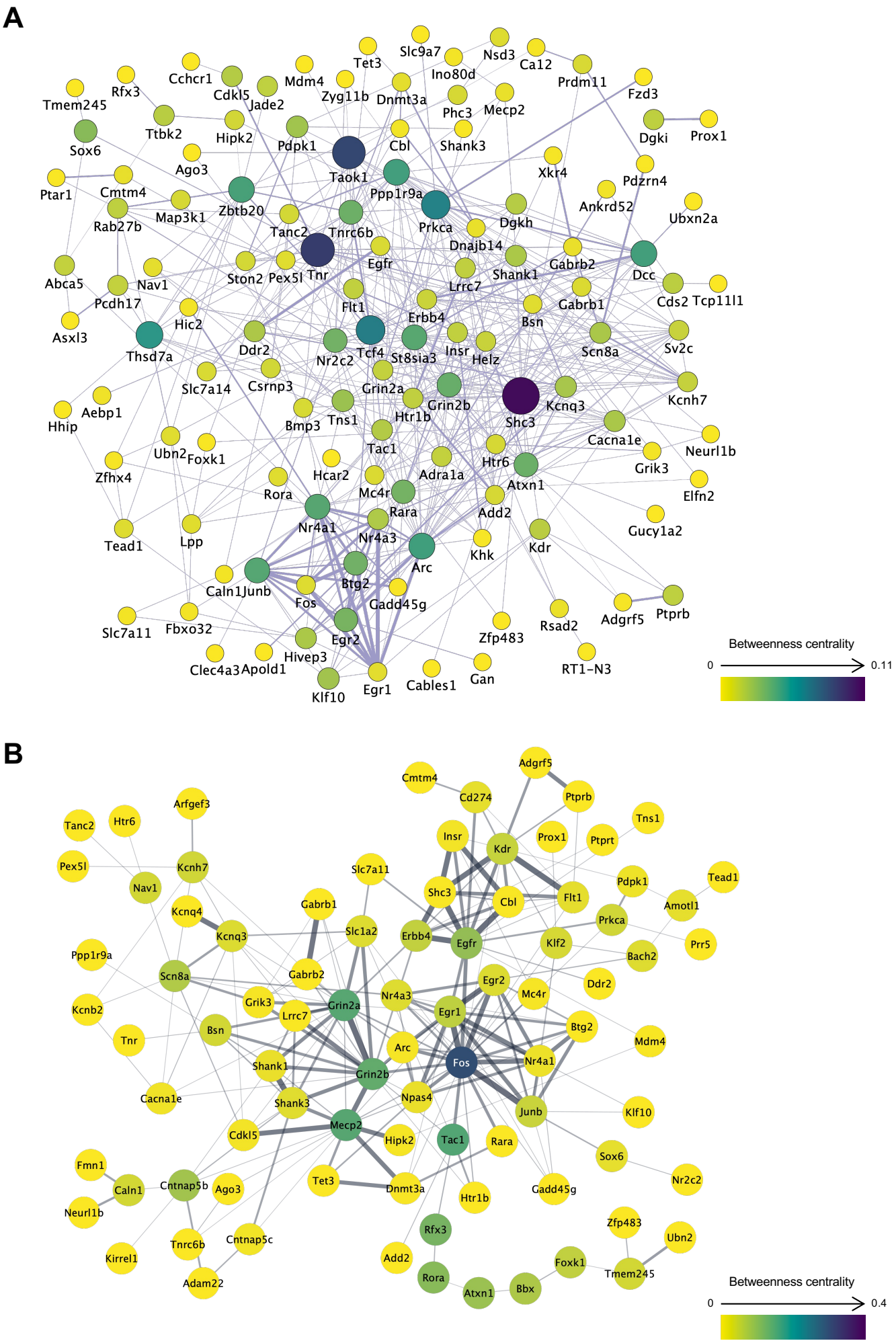
A
Tmem245
Rfx3
Cchcr1
Cdkl5
Jade2
Mdm4
Zyg11b
Tet3
Slc9a7
Ino80d
Nsd3
Ca12
Prdm11
Fzd3
Dnmt3a
Phc3
Mecp2
Dgki
Prox1
Sox6
Ttbk2
Hipk2
Pdpk1
Cbl
Shank3
Ago3
Taok1
Xkr4
Pdzrn4
Ptar1
Cmtm4
Ppp1r9a
Ankrd52
Ubxn2a
Rab27b
Map3k1
Zbtb20
Tanc2
Tnrc6b
Prkca
Dgkh
Dnajb14
Abca5
Nav1
Egfr
Gabrb2
Dcc
Pcdh17
Ston2
Pex5l
Tnr
Shank1
Lrrc7
Cds2
Tcp11l1
Asxl3
Hic2
Flt1
Erbb4
Gabrb1
Bsn
Thsd7a
Ddr2
Nr2c2
Tcf4
St8sia3
Insr
Helz
Scn8a
Sv2c
Slc7a14
Csrnp3
Grin2a
Grin2b
Kcnq3
Kcnh7
Aebp1
Hhip
Bmp3
Tns1
Htr1b
Shc3
Cacna1e
Neurl1b
Ubn2
Foxk1
Tac1
Htr6
Grik3
Zfhx4
Hcar2
Adra1a
Atxn1
Elfn2
Rora
Mc4r
Rara
Add2
Gucy1a2
Nr4a1
Nr4a3
Tead1
Lpp
Khk
Kdr
Arc
Caln1
Junb
Btg2
Fos
Gadd45g
Slc7a11
Fbxo32
Egr2
Zfp483
Rsad2
Adgrf5
Ptprb
Hivep3
Clec4a3
Apold1
Egr1
Cables1
Gan
RT1-N3
Klf10
Betweenness centrality
0
0.11
B
Adgrf5
Cmtm4
Cd274
Ptprb
Arfgef3
Tanc2
Htr6
Tns1
Insr
Kdr
Prox1
Ptprt
Pex5l
Kcnh7
Slc7a11
Nav1
Shc3
Cbl
Flt1
Pdpk1
Tead1
Kcnq4
Gabrb1
Amotl1
Prkca
Kcnq3
Slc1a2
Erbb4
Egfr
Klf2
Prr5
Ppp1r9a
Bach2
Scn8a
Gabrb2
Egr2
Ddr2
Kcnb2
Grik3
Nr4a3
Mc4r
Lrrc7
Grin2a
Egr1
Btg2
Tnr
Bsn
Arc
Mdm4
Shank1
Fos
Nr4a1
Grin2b
Cacna1e
Shank3
Npas4
Junb
Klf10
Cdkl5
Mecp2
Hipk2
Tac1
Rara
Sox6
Fmn1
Caln1
Cntnap5b
Ago3
Tet3
Dnmt3a
Htr1b
Gadd45g
Nr2c2
Neurl1b
Zfp483
Rfx3
Ubn2
Tnrc6b
Cntnap5c
Kirrel1
Add2
Foxk1
Tmem245
Adam22
Rora
Atxn1
Bbx
Betweenness centrality
0
0.4

Fig 6

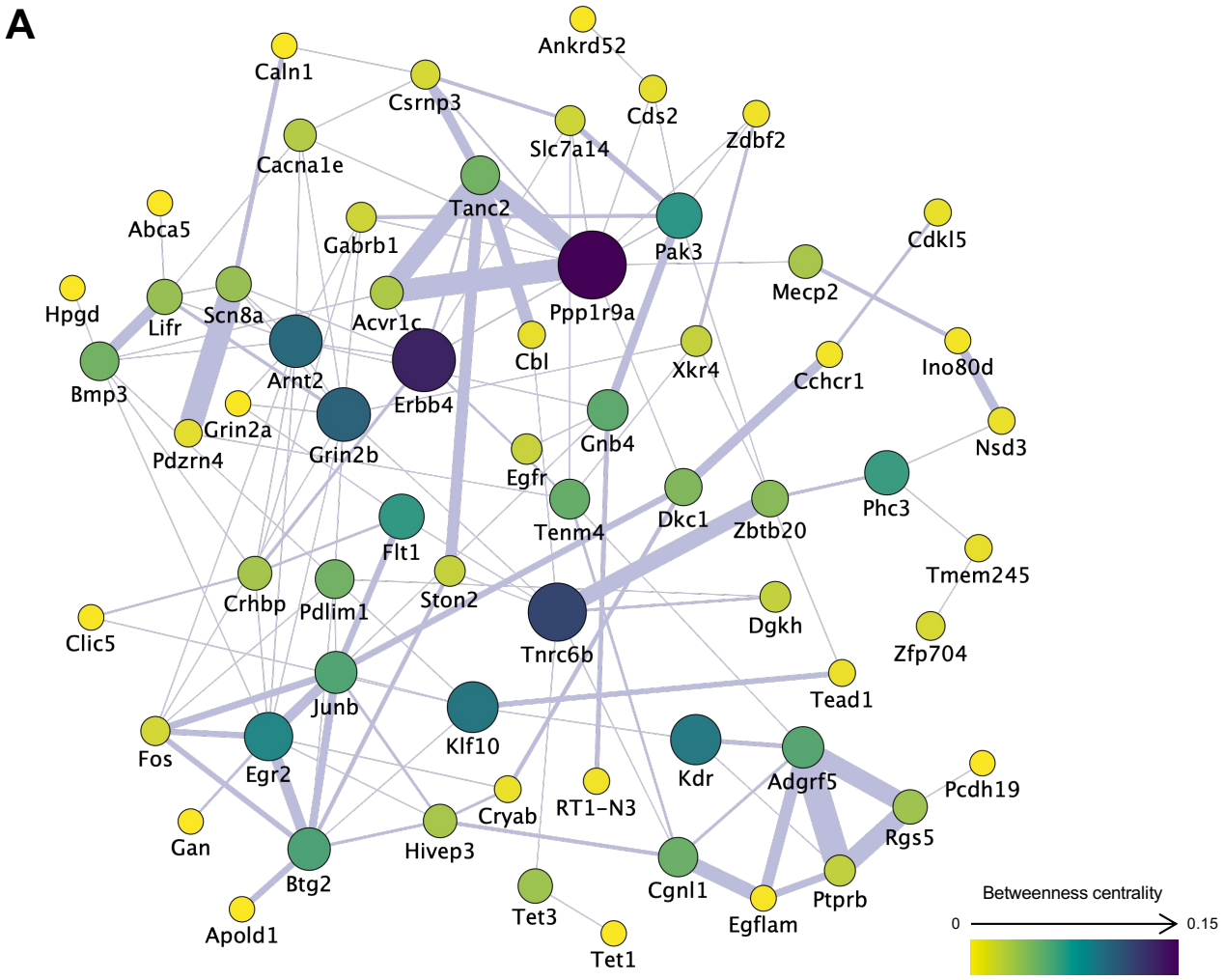
A
Ankrd52
Caln1
Csrnp3
Cds2
Zdbf2
Slc7a14
Cacna1e
Tanc2
Abca5
Gabrb1
Pak3
Cdkl5
Mecp2
Hpgd
Lifr
Scn8a
Acvr1c
Ppp1r9a
Cbl
Xkr4
Cchcr1
Ino80d
Bmp3
Arnt2
Erbb4
Grin2a
Grin2b
Gnb4
Nsd3
Pdzrn4
Egfr
Phc3
Tenm4
Dkc1
Zbtb20
Flt1
Tmem245
Crhbp
Pdlim1
Ston2
Dgkh
Clic5
Tnrc6b
Zfp704
Junb
Tead1
Klf10
Fos
Egr2
Kdr
Adgrf5
Pcdh19
Cryab
RT1-N3
Rgs5
Gan
Hivep3
Btg2
Cgnl1
Ptprb
Tet3
Egflam
Apold1
Tet1
Betweenness centrality
0
0.15

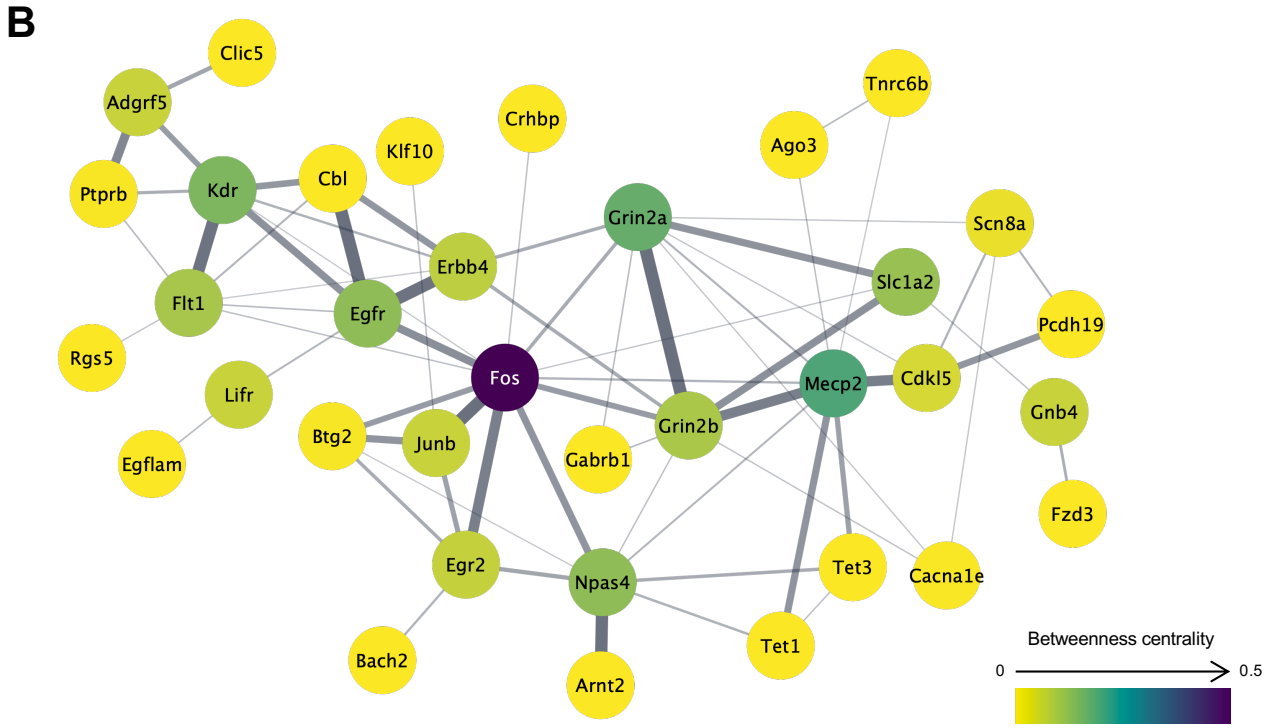
B
Clic5
Tnrc6b
Adgrf5
Crhbp
Ago3
Klf10
Ptprb
Kdr
Cbl
Grin2a
Scn8a
Erbb4
Slc1a2
Flt1
Egfr
Pcdh19
Rgs5
Fos
Mecp2
Cdkl5
Lifr
Gnb4
Grin2b
Btg2
Junb
Gabrb1
Egflam
Fzd3
Egr2
Npas4
Tet3
Cacna1e
Tet1
Bach2
Arnt2
Betweenness centrality
0
0.5

Fig 7

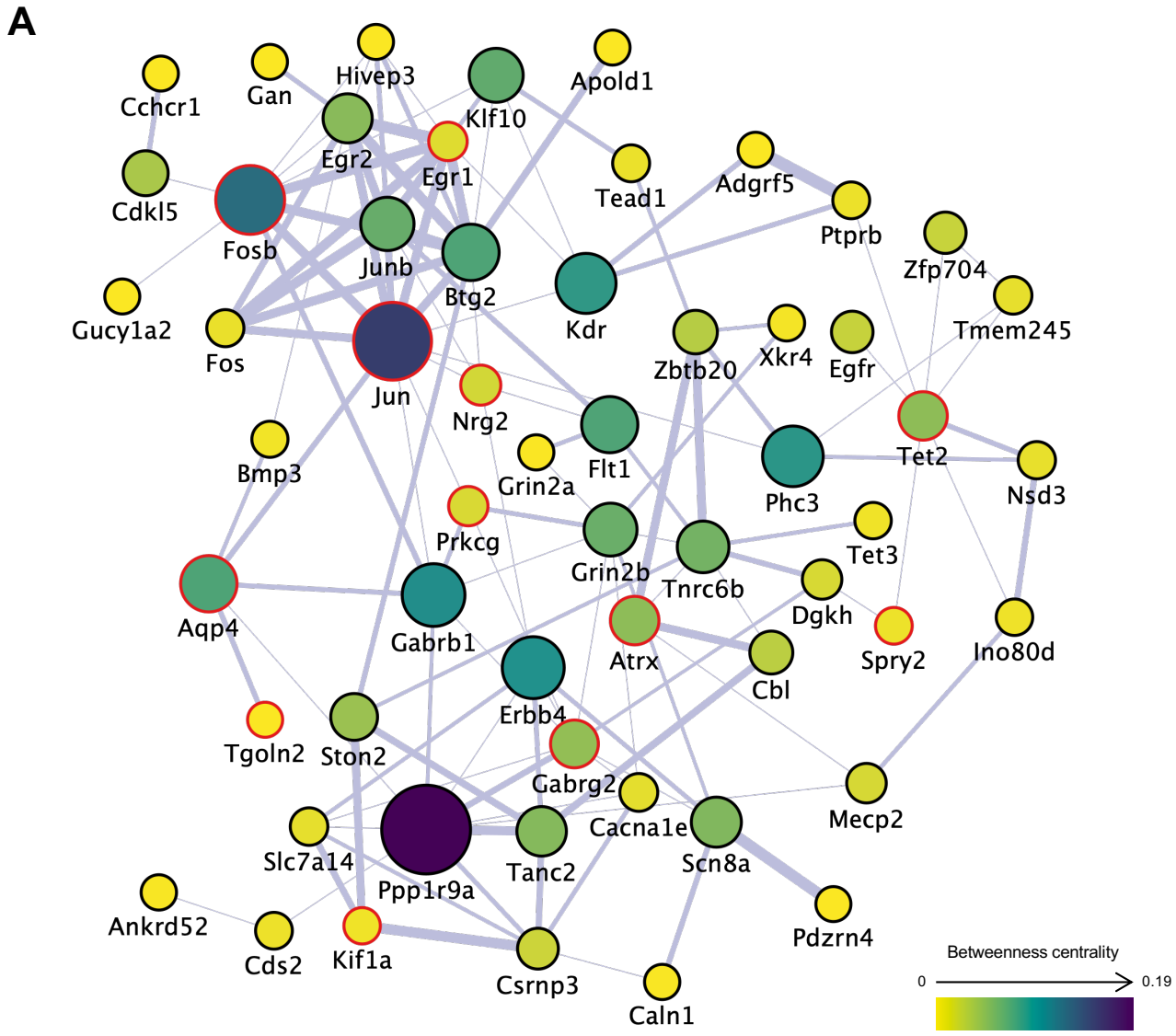
A
Cchcr1
Gan
Hivep3
Klf10
Apold1
Egr2
Egr1
Cdkl5
Fosb
Tead1
Adgrf5
Ptprb
Zfp704
Junb
Btg2
Kdr
Gucy1a2
Fos
Jun
Zbtb20
Xkr4
Egfr
Tmem245
Nrg2
Bmp3
Grin2a
Flt1
Tet2
Phc3
Nsd3
Prkcg
Grin2b
Tnrc6b
Tet3
Aqp4
Gabrb1
Dgkh
Atrx
Spry2
Ino80d
Cbl
Erbb4
Tgoln2
Ston2
Gabrg2
Cacna1e
Mecp2
Slc7a14
Ppp1r9a
Tanc2
Scn8a
Ankrd52
Cds2
Kif1a
Pdzrn4
Csrnp3
Caln1
Betweenness centrality
0
0.19

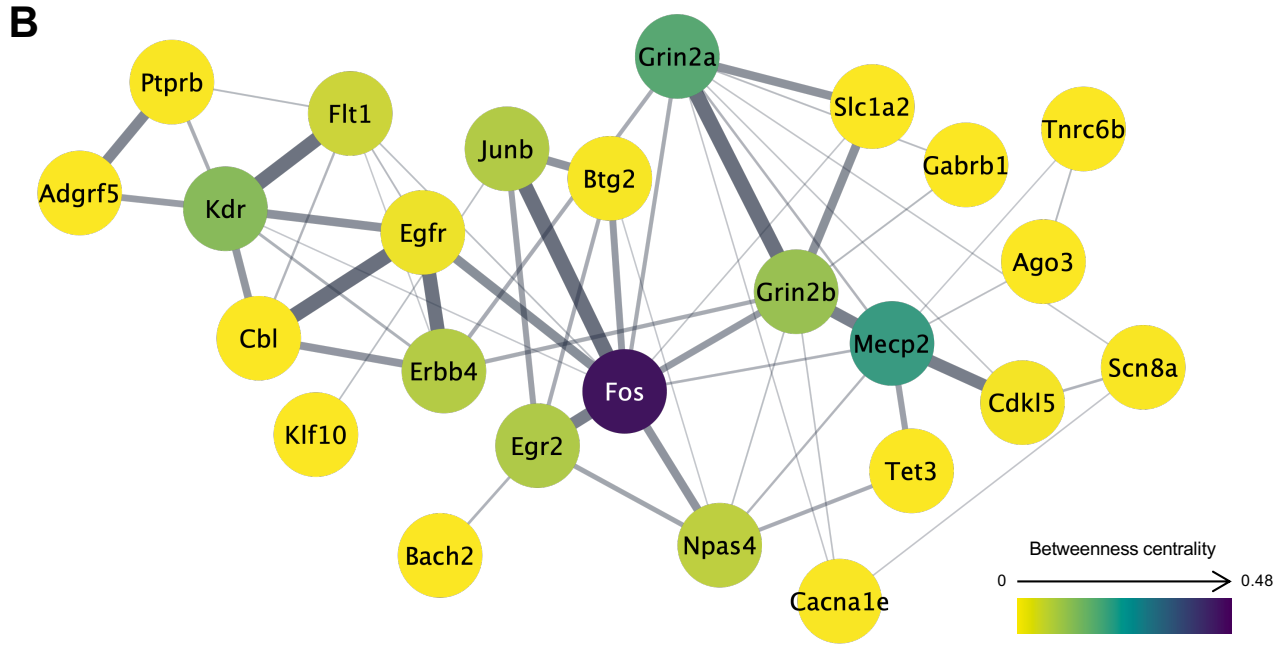
B
Grin2a
Ptprb
Flt1
Slc1a2
Tnrc6b
Junb
Gabrb1
Adgrf5
Kdr
Btg2
Egfr
Ago3
Grin2b
Cbl
Mecp2
Scn8a
Erbb4
Fos
Cdkl5
Klf10
Egr2
Tet3
Bach2
Npas4
Cacna1e
Betweenness centrality
0
0.48

Fig 8

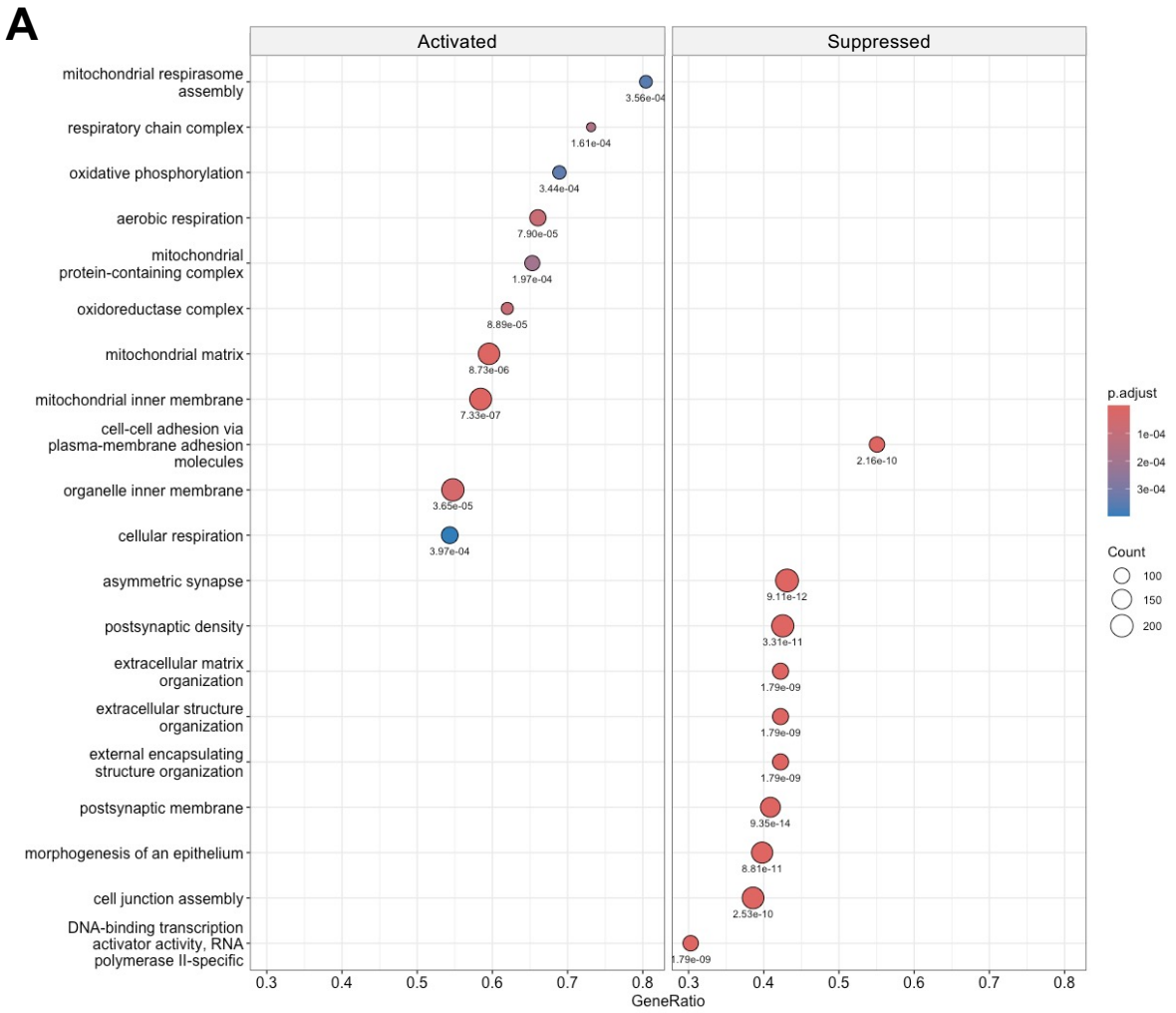
A
Activated
Suppressed
mitochondrial respirasome assembly
respiratory chain complex
oxidative phosphorylation
aerobic respiration
mitochondrial protein-containing complex
oxidoreductase complex
mitochondrial matrix
mitochondrial inner membrane
cell-cell adhesion via plasma-membrane adhesion molecules
organelle inner membrane
cellular respiration
asymmetric synapse
postsynaptic density
extracellular matrix organization
extracellular structure organization
external encapsulating structure organization
postsynaptic membrane
morphogenesis of an epithelium
cell junction assembly
DNA-binding transcription activator activity, RNA polymerase II-specific
3.56e-04
1.61e-04
3.44e-04
7.90e-05
1.97e-04
8.89e-05
8.73e-06
7.33e-07
3.65e-05
3.97e-04
2.16e-10
9.11e-12
3.31e-11
1.79e-09
1.79e-09
1.79e-09
9.35e-14
8.81e-11
2.53e-10
1.79e-09
0.3 0.4 0.5 0.6 0.7 0.8
GeneRatio
p.adjust
1e-04
2e-04
3e-04
Count
100
150
200

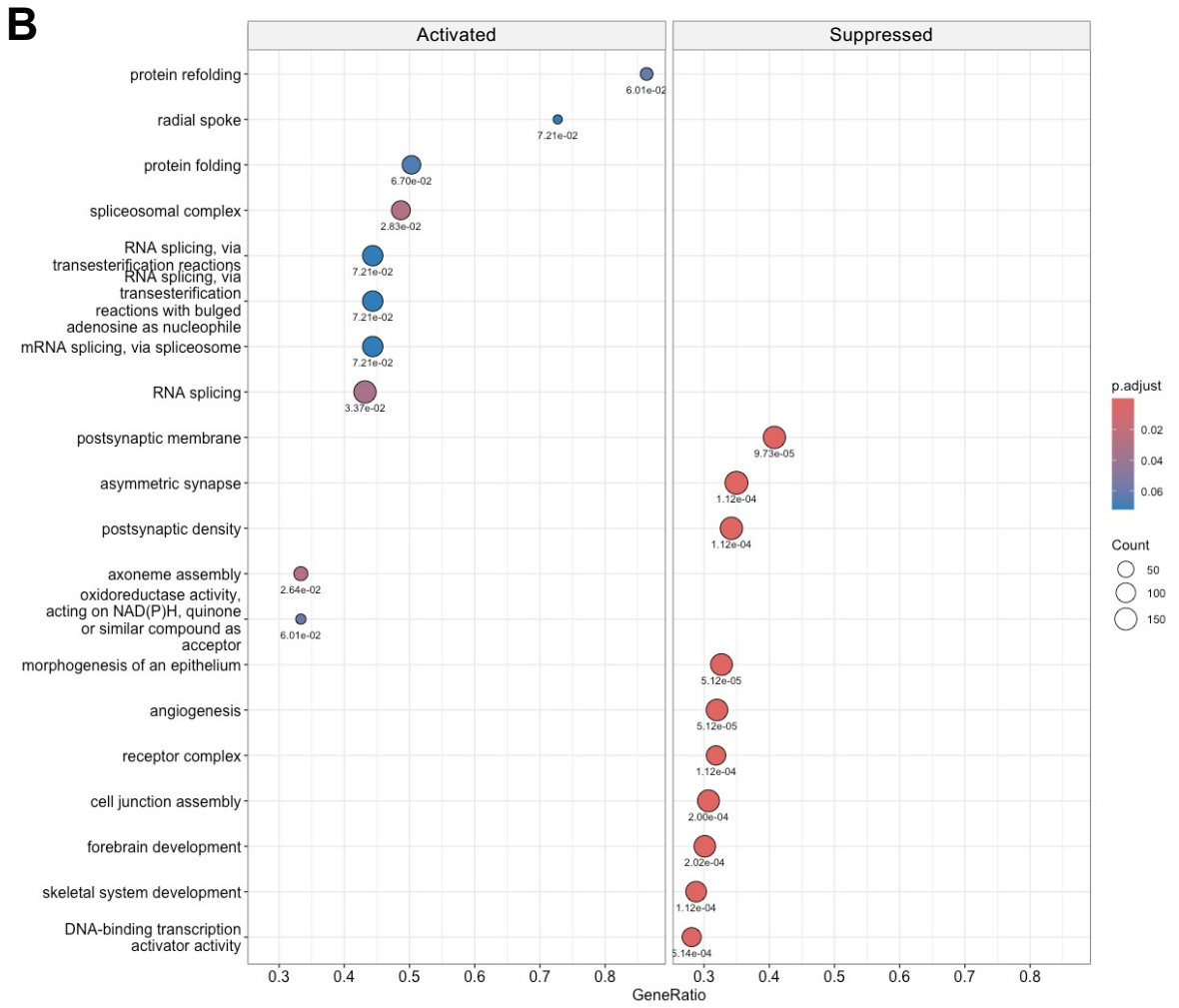
B
Activated
Suppressed
protein refolding
radial spoke
protein folding
spliceosomal complex
RNA splicing, via transesterification reactions
RNA splicing, via transesterification reactions with bulged adenosine as nucleophile
mRNA splicing, via spliceosome
RNA splicing
postsynaptic membrane
asymmetric synapse
postsynaptic density
axoneme assembly
oxidoreductase activity, acting on NAD(P)H, quinone or similar compound as acceptor
morphogenesis of an epithelium
angiogenesis
receptor complex
cell junction assembly
forebrain development
skeletal system development
DNA-binding transcription activator activity
6.01e-02
7.21e-02
6.70e-02
2.83e-02
7.21e-02
7.21e-02
7.21e-02
3.37e-02
9.73e-05
1.12e-04
1.12e-04
2.64e-02
6.01e-02
5.12e-05
5.12e-05
1.12e-04
2.00e-04
2.02e-04
1.12e-04
5.14e-04
0.3 0.4 0.5 0.6 0.7 0.8
GeneRatio
p.adjust
0.02
0.04
0.06
Count
50
100
150